Journal of Geochemical Exploration 233 (2022) 106922

Contents lists available at ScienceDirect

Journal of Geochemical Exploration

journal homepage: www.elsevier.com/locate/gexplo

Hierarchical clustering and compositional data analysis for interpreting groundwater hydrogeochemistry: The application to Campi Flegrei volcanic aquifer (south Italy)

Pooria Ebrahimi [a,*], Annalise Guarino [a], Vincenzo Allocca [a], Stefano Caliro [b], Rosario Avino [b], Emanuela Bagnato [b], Francesco Capecchiacci [b,c], Antonio Carandente [b], Carmine Minopoli [b], Alessandro Santi [b], Stefano Albanese [a]

[a] Department of Earth, Environmental and Resources Sciences, University of Naples Federico II, Naples 80126, Italy
[b] Istituto Nazionale di Geofisica e Vulcanologia, Sezione di Napoli, "Osservatorio Vesuviano", Naples 80124, Italy
[c] Department of Earth Sciences, University of Florence, Florence 50121, Italy

ARTICLE INFO

Keywords:
Hierarchical cluster analysis
Groundwater evolution
Hydrothermal system
Precursors of volcanic eruption
Compositional nature of data
Mixing process

ABSTRACT

Comprehensive hydrogeochemical studies have been conducted in the Campi Flegrei volcanic aquifer since late 20th century due to the volcanic unrest. In the last decade, groundwater samples were grouped based on the dominant anion species (i.e. bicarbonate, sulfate and chloride) to explain the general hydrogeochemical processes. In this article, 44 groundwater samples are collected from Campi Flegrei aquifer to geochemically and spatially capture the main characteristics of the groundwater body. The hierarchical clustering algorithm is then performed on proportion of bicarbonate, sulfate and chloride, and the optimum number of clusters are determined regarding the results of deep hydrogeochemical investigations published in the past. The collected samples are categorized in the following groups: (1) bicarbonate-rich groundwater; (2) chlorine-rich groundwater; (3) sulfate-rich groundwater; and (4) mixed groundwater. The first group (As = 158.2 ± 169 μg/l, electric conductivity = 1,732.1 ± 1,086 μS/cm and temperature = 25.6 ± 8 °C) is mainly derived from poor arsenic meteoric water, but there is significant thermal/seawater contribution in the second one (As = 1,457.8 ± 2,210 μg/l, electric conductivity = 20,118.3 ± 11,139 μS/cm and temperature = 37.1 ± 20 °C). Interaction of the bicarbonate-rich groundwater and hydrothermal vapors gives rise to the sulfate-rich groundwater (As = 847.2 ± 679 μg/l, electric conductivity = 3,940.0 ± 540 μS/cm and temperature = 82.8 ± 3 °C) around Solfatara volcano. The mixed groundwater (As = 451.4 ± 388 μg/l, electric conductivity = 4,482.9 ± 4,027 μS/cm and temperature = 37.1 ± 16 °C) is observed where the three main groundwater groups undergo a mixing process, depending on the hydrogeology of the volcanic aquifer. Contrary to the bicarbonate- and sulfate-rich groundwater, the chlorine-rich and mixed groundwater generally occurs at low piezometric levels (approximately <1 m above sea level) near the coastline. The hierarchical cluster analysis provides more information about the volcanic aquifer, particularly when compositional data analysis is applied to study hydrogeochemistry of the homogeneous groundwater groups and to uncover the relationships between variables. Addressing compositional nature of data is recommended in the future studies for developing new tools that help deeper understanding of groundwater evolution in volcanic aquifers and identifying promising precursors of volcanic eruption.

1. Introduction

Geothermal activities occur in the areas of active volcanism, continental collision zones, continental rift systems associated with active volcanism, as well as continental rifts not associated with volcanoes (Chandrasekharam and Bundschuh, 2002; Moeck, 2014). A wide range of secondary processes affect chemical composition of the rising geothermal fluids from the reservoir to the surface. In coastal areas, thermal fluids are generally brackish to saline Na–Cl type because seawater alters the original chemical characteristics of the fluids (Dotsika, 2015). Different extents of mixing process between meteoric water, geothermal fluids and steam results in various hydrogeochemical

* Corresponding author.
E-mail addresses: pooria.ebrahimi@unina.it, pooria.ebrahimi@gmail.com (P. Ebrahimi).

https://doi.org/10.1016/j.gexplo.2021.106922
Received 7 June 2021; Received in revised form 7 November 2021; Accepted 26 November 2021
Available online 1 December 2021

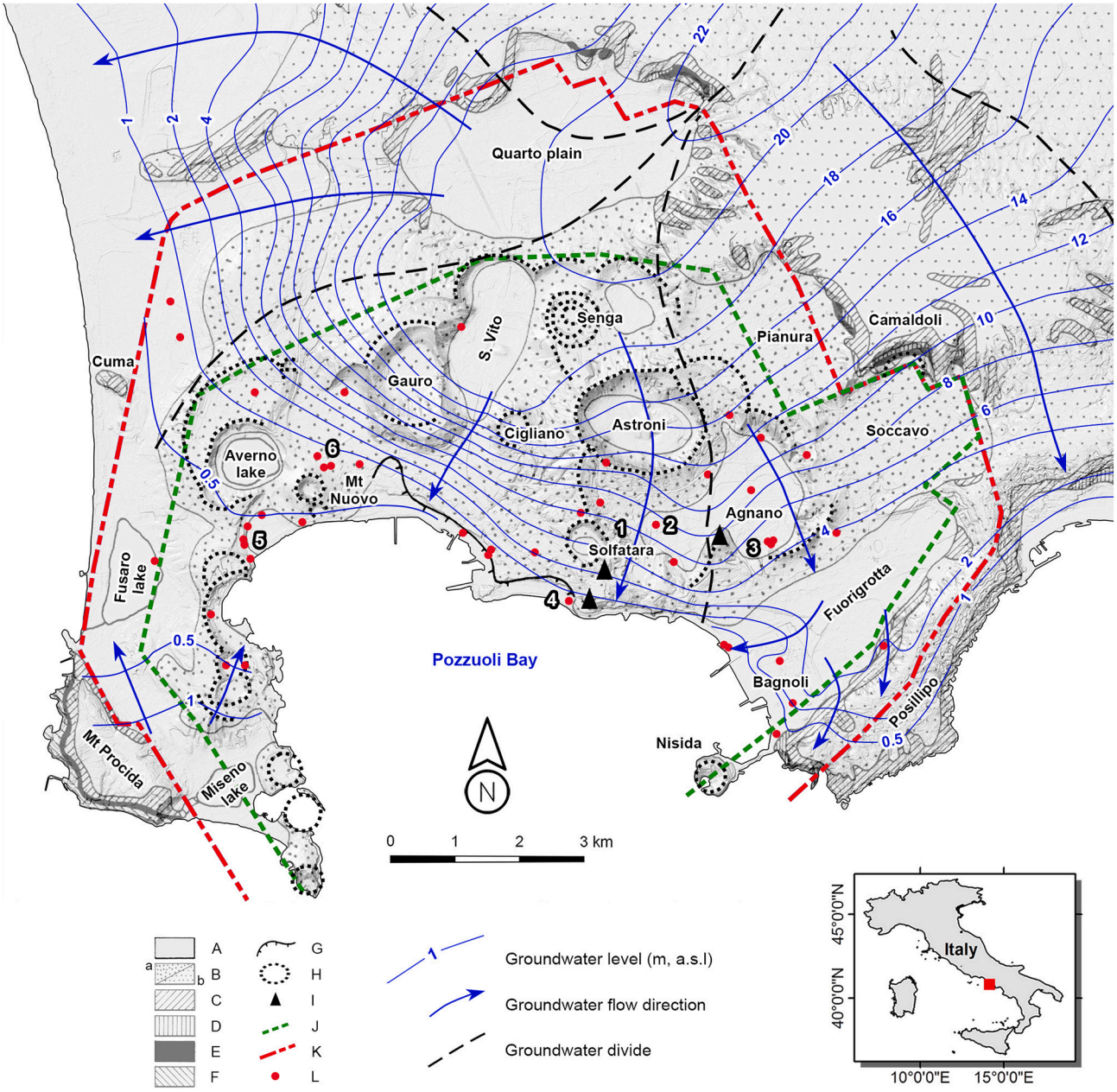

Fig. 1. The simplified geological map of Campi Flegrei (after Valentino et al., 1999). The groundwater level, groundwater flow direction, groundwater divide (after De Vita et al., 2018) together with location of (1) Pisciarelli, (2) Hotel Tennis, (3) Agnano Terme, (4) Terme Puteolane, (5) Stufe di Nerone and (6) Damiani are also represented. Legend: (A) Recent active continental sediments; (B) Volcanics younger than 12 ka: (a) proximal, mostly pyroclastic-flow and surge deposits, (b) distal, mostly fallout deposits; (C) Neapolitan Yellow Tuff (NYT; 12 ka B.P.); (D) Volcanics erupted 35–12 ka B.P.; (E) Campanian Ignimbrite (CI; 35 ka B.P.); (F) Volcanics older than 35 ka; (G) Edge of La Starza marine cliff; (H) Crater rims of volcanoes younger than 12 ka (ISPRA, 2018); (I) Lava domes; (J) NYT caldera rim (Vitale and Isaia, 2014); (K) CI caldera rim (Vitale and Isaia, 2014); and (L) sampling points.

signatures. Delineating these signals provides some information about evolution of the hydrothermal system, geothermal exploration and volcanic activity.

Campi Flegrei is one of the most active volcanic areas in the world, well-known for the striking ground movements or bradyseism, in which thermal energy is mainly released through diffuse degassing (Chiodini et al., 2001). Groundwater hydrogeochemistry was extensively investigated in the Campi Flegrei volcanic aquifer before 2007 (Aiuppa et al., 2006; Avino et al., 1999; Capaldi et al., 1992; Celico et al., 1992; Valentino et al., 1999; Valentino and Stanzione, 2003, 2004), but recent studies focused on specific sectors of the aquifer such as Bagnoli–Fuorigrotta Plain (Arienzo et al., 2015; De Vivo and Lima, 2008), Agnano Plain, Solfatara volcano (Bagnato et al., 2009) and Cuma (Allocca et al., 2018; Stellato et al., 2020). Noticeable groundwater heterogeneity likely reflects inhomogeneous water discharge, various residence times of groundwater in the aquifer and/or spatially variable contributions from deep thermal fluids (Aiuppa et al., 2006).

Since the beginning of this century, Campi Flegrei showed signs of volcanic unrest (Chiodini et al., 2010, 2012): changes in behavior of the volcanic system, composition of fumarolic gases and frequency of earthquake swarms. These observations are indicators of higher magmatic component and ground uplift which raised concerns of the scientific community about volcanic reawakening. The Campi Flegrei caldera and the surrounding environment have been highly populated since the ancient Greek times. In this region, cities (e.g., Naples, Pozzuoli and Cuma) form a seamless urban area with more than 2 million

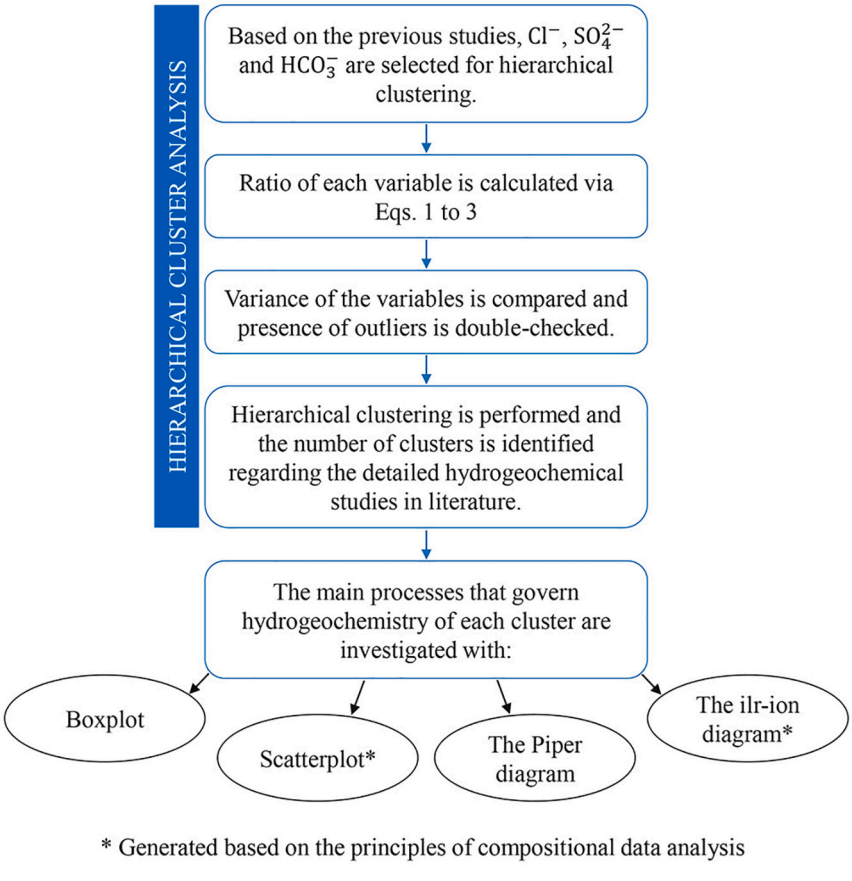

Fig. 2. The flowchart demonstrating the main data treatment and visualization steps.

inhabitants (Giudicepietro et al., 2019). Hence, there is a need to better understand the present volcanic unrest and to be prepared for a possible emergency. To evaluate volcanic hazards, geochemical tracers provide unique information about spatial distribution and temporal rate of magma degassing along with activity of the magma chamber. However, hydrogeochemical assessment of volcanic aquifers situated in densely populated coastal areas is challenging because many factors affect groundwater chemistry.

Geochemical data are regularly reported as proportions such as weight percentages (wt%), milligrams per liter (mg/l) and micrograms per liter (μg/l). It means that such data subject to a constant sum because each component explains only a part of the whole composition. Karl Pearson introduced the problem of spurious correlation in this type of data (Pearson, 1897) and applying statistical analysis to compositional data has been an issue for more than a century. Compositional data analysis refers to a family of log-ratio transformations which was introduced by Aitchison (1982) and Egozcue et al. (2003) for converting the compositional data from their original sample space to an unrestricted real space. It has attracted attention of many researchers (Buccianti and Grunsky, 2014; Dominech et al., 2021, 2022; Ebrahimi et al., 2021) because the ratios between compositional parts are much more informative for understanding the complex geochemical data structure. To the best of our knowledge, it has not been used for studying hydrothermal systems and groundwater geochemistry in volcanic areas. The main objective of this work is taking advantage of the long history of hydrogeochemical research in the study area to apply hierarchical cluster analysis (HCA) and compositional data analysis for investigating groundwater geochemistry, which might provide new tools for monitoring volcanic activity more accurately and mitigating risk of volcanic eruption more effectively.

2. Study area

The volcanic system of Campi Flegrei is located in an area of extensive tectonic activity on the Tyrrhenian coast, south Italy (Fig. 1). It covers an area of ca. 200 km^2 (Sellerino et al., 2019) with the maximum elevation of about 250 m above sea level. Distribution of the volcanic centers was controlled by NE-SW and NW-SE faults in the study area. The volcanic activity began before 80 ka (Neapolitan volcanoes; Scarpati et al., 2013) and the last eruption (Monte Nuovo) occurred in 1538 CE. The majority of these volcanic eruptions were explosive (Vitale and Isaia, 2014). Campanian Ignimbrite (CI: 35 ka B.P.) and Neapolitan Yellow Tuff (NYT: 12 ka B.P.) eruptions led to formation of the present 12-km wide caldera (Aiuppa et al., 2006). Varying from trachybasalts to phonolitic and peralkaline trachytes in composition (Armienti et al., 1983; Di Girolamo, 1978), the volcanic products of Campi Flegrei can be considered as a part of the potassium-rich Roman comagmatic province in central-southern Italy (Peccerillo, 1985; Washington, 1906). Recent active continental sediments and volcanic deposits younger than 12 ka covered the area and the older outcrops occurred around the NYT and CI caldera rims (Fig. 1). The fumaroles in the Pozzuoli Bay and Solfatara volcano along with the hot springs and steam-heated pools indicate intense hydrothermal activity in the study area (Aiuppa et al., 2006).

Since the middle of the last century, the caldera experienced a long-term bradyseismic crisis associated with temporal injections of CO_2-rich magmatic fluids at the bottom of the hydrothermal system (Caliro et al., 2007). This resulted in periodic ground uplifts and seismic activities with a maximum total uplift of approximately 4 m from 1983 to 1984 (Del Gaudio et al., 2010). It followed an episode of subsidence until 2004–2005 when another uplift phase began. From 2012 to 2013, deformation rate was accelerated (D'Auria et al., 2015; Trasatti et al., 2015) due to magma emplacement at shallow depth (D'Auria et al.,

Table 1
The measured values of ions, elements and physico-chemical parameters in Campi Flegrei groundwater samples.

ID	Groundwater type	Dominant anion group[a]	HCA group[b]	Ca^{2+}	Mg^{2+}	Na^{+}	K^{+}	Cl^{-}	SO_4^{2-}	HCO_3^{-}	NO_3^{-}	F^{-}	Li	As	B	EC	T	pH
W1	Na–SO_4	SGW	$C4_{SGW}$	38.3	0.4	768.0	184.0	126.0	1,040.0	817.0	0.7	9.6	423.0	168.1	1,457.5	3,400	86.2	7.0
W2	Na–SO_4	SGW	$C4_{SGW}$	89.2	2.0	1,000.0	288.0	119.0	1,880.0	987.0	<D.L.	3.1	629.0	1,526.3	27,900.0	4,480	79.4	6.8
W3	Ca–Cl	ClGW	$C2_{MGW}$	131.0	13.9	135.0	53.4	214.0	223.0	216.0	138.0	1.2	<D.L.	14.4	314.4	1,420	16.4	6.9
W4	Na–Cl	ClGW	$C2_{MGW}$	34.9	7.3	482.0	133.0	413.0	205.0	492.0	101.0	7.3	290.0	460.1	1,040.0	2,550	36.0	7.7
W5	Na–Cl	ClGW	$C3_{ClGW}$	164.0	11.4	7,740.0	176.0	10,900.0	1,410.0	2,260.0	<D.L.	1.3	11,000.0	3.2	88,812.5	23,000	20.0	6.2
W6	Na–Cl	ClGW	$C2_{MGW}$	65.6	10.4	261.0	53.2	316.0	115.0	374.0	45.9	4.4	149.0	168.9	938.4	1,690	21.3	7.1
W7	Na–Cl	ClGW	$C2_{MGW}$	37.1	3.1	542.0	113.0	511.0	204.0	474.0	104.0	7.7	275.0	419.5	5,378.8	2,650	44.3	7.3
W8	Na–Cl	ClGW	$C2_{MGW}$	263.0	57.0	2,020.0	327.0	2,880.0	376.0	1,300.0	2.8	2.1	1,230.0	322.5	13,837.5	8,110	56.0	6.6
W9	Na–Cl	ClGW	$C2_{MGW}$	82.1	2.9	495.0	115.0	417.0	254.0	478.0	129.0	6.0	312.0	506.9	1,656.3	2,480	35.9	7.8
W10	Na–Cl	ClGW	$C3_{ClGW}$	564.0	872.0	11,200.0	761.0	20,700.0	2,240.0	807.0	7.9	2.4	4,410.0	3,538.8	23,800.0	37,000	67.0	6.1
W11	Na–Cl	ClGW	$C3_{ClGW}$	382.0	244.0	7,870.0	539.0	14,800.0	317.0	48.8	1.2	6.0	4,210.0	<D.L.	9,927.5	33,100	43.7	6.5
W12	Na–Cl	ClGW	$C3_{ClGW}$	182.0	12.8	3,850.0	250.0	6,330.0	200.0	810.0	65.6	2.7	6,660.0	1,610.0	10,470.0	14,780	29.5	6.5
W13	Na–Cl	ClGW	$C2_{MGW}$	59.6	0.7	1,070.0	378.0	932.0	1,090.0	758.0	0.7	3.8	645.0	968.9	19,825.0	5,160	75.0	7.3
W14	Na–Cl	ClGW	$C3_{ClGW}$	85.0	9.8	108.0	20.6	349.0	7.2	83.0	4.3	0.4	<D.L.	11.9	191.3	795	18.3	7.2
W15	Ca–Cl	ClGW	$C2_{MGW}$	209.0	4.7	212.0	30.2	234.0	267.0	262.0	174.0	4.5	<D.L.	333.5	2,888.8	17,160	36.4	7.5
W16	Na–Cl	ClGW	$C2_{MGW}$	21.0	0.9	232.0	37.3	234.0	27.6	299.0	<D.L.	12.7	<D.L.	158.9	1,407.5	1,230	–	7.6
W17	Na–Cl	ClGW	$C2_{MGW}$	63.0	12.0	559.0	493.0	916.0	343.0	580.0	1.1	9.5	<D.L.	118.6	3,170.0	2,310	26.4	5.7
W18	Na–Cl	ClGW	$C2_{MGW}$	424.0	31.4	1,690.0	282.0	2,230.0	368.0	1,190.0	1.7	1.8	329.0	524.6	7,246.3	5,600	21.4	6.4
W19	Na–Cl	ClGW	$C3_{ClGW}$	516.0	526.0	7,110.0	829.0	12,600.0	1,560.0	1,620.0	1.7	3.0	2,610.0	23.2	11,098.8	25,500	18.7	6.0
W20	Na–Cl	ClGW	$C2_{MGW}$	99.0	8.4	503.0	95.9	586.0	139.0	586.0	12.8	5.8	295.0	258.3	5,226.3	2,680	23.5	7.6
W21	Na–Cl	ClGW	$C2_{MGW}$	127.0	30.0	843.0	143.0	931.0	134.0	1,150.0	16.0	2.9	264.0	473.8	7,005.0	3,380	36.2	6.9
W22	Na–Cl	ClGW	$C3_{ClGW}$	309.0	60.5	7,370.0	207.0	11,000.0	611.0	371.0	132.0	13.7	11,400.0	6,875.0	31,700.0	26,000	77.0	6.9
W23	Na–Cl	ClGW	$C3_{ClGW}$	168.0	77.9	2,430.0	208.0	3,990.0	405.0	870.0	33.0	6.0	2,380.0	793.6	13,975.0	11,490	32.0	7.0
W24	Na–Cl	ClGW	$C3_{ClGW}$	188.0	29.0	2,070.0	148.0	3,560.0	194.0	336.0	80.9	2.4	2,330.0	262.9	6,111.3	9,400	27.3	7.1
W25	Na–HCO_3	BGW	$C1_{BGW}$	58.8	7.9	212.0	69.3	100.0	129.0	309.0	65.3	4.9	<D.L.	41.5	595.1	1,021	21.0	7.4
W26	Na–HCO_3	BGW	$C1_{BGW}$	317.0	26.1	498.0	138.0	510.0	613.0	1,000.0	0.4	0.4	363.0	724.4	16,587.5	2,770	40.5	6.2
W27	Na–HCO_3	BGW	$C1_{BGW}$	180.0	68.4	637.0	99.4	551.0	430.0	1,130.0	355.0	3.1	196.0	33.6	1,058.9	3,770	22.7	7.1
W28	Na–HCO_3	BGW	$C1_{BGW}$	99.9	9.3	116.0	50.8	88.9	195.0	265.0	101.0	4.1	<D.L.	34.5	425.7	787	17.5	7.4
W29	Na–HCO_3	BGW	$C1_{BGW}$	42.0	5.8	246.0	102.0	153.0	89.1	614.0	73.4	1.3	<D.L.	199.6	334.1	1,550	25.1	7.2
W30	Na–HCO_3	BGW	$C1_{BGW}$	127.0	7.3	147.0	75.0	129.0	228.0	295.0	168.0	6.7	<D.L.	44.2	252.1	1,360	17.4	7.4
W31	Na–HCO_3	BGW	$C1_{BGW}$	162.0	17.4	724.0	134.0	179.0	256.0	1,870.0	0.6	3.1	883.0	154.8	1,776.3	2,490	26.0	6.8
W32	Na–HCO_3	BGW	$C1_{BGW}$	31.5	1.9	263.0	35.1	162.0	67.8	447.0	50.1	9.2	<D.L.	73.5	781.0	1,340	22.3	7.6
W33	Na–HCO_3	BGW	$C1_{BGW}$	118.0	29.9	823.0	110.0	412.0	247.0	1,700.0	7.7	2.2	980.0	292.4	4,681.3	3,200	35.7	6.3
W34	Na–HCO_3	BGW	$C1_{BGW}$	149.0	26.7	764.0	136.0	462.0	148.0	1,590.0	0.6	3.2	770.0	166.4	5,713.8	3,060	33.3	6.4
W35	Na–HCO_3	BGW	$C1_{BGW}$	3.7	0.1	299.0	36.5	174.0	7.9	509.0	0.4	12.3	<D.L.	234.6	2,432.5	1,218	32.8	8.6
W36	Na–HCO_3	BGW	$C1_{BGW}$	57.1	2.3	90.1	54.8	69.5	127.0	238.0	10.3	7.5	<D.L.	28.1	943.4	633	16.7	7.8
W37	Na–HCO_3	BGW	$C1_{BGW}$	32.2	2.3	43.8	41.4	28.3	5.1	204.0	0.8	1.9	<D.L.	6.9	1,666.0	350	19.1	8.1
W38	Ca–HCO_3	BGW	$C1_{BGW}$	215.0	9.0	132.0	76.4	140.0	254.0	512.0	176.0	3.6	<D.L.	72.3	964.3	1,159	18.8	7.3
W39	Na–HCO_3	BGW	$C2_{MGW}$	39.4	5.1	1,690.0	157.0	1,100.0	530.0	1,940.0	24.1	3.7	928.0	1,590.0	13,437.5	6,340	53.4	6.9
W40	Na–HCO_3	BGW	$C1_{BGW}$	107.0	17.9	400.0	100.0	259.0	205.0	926.0	0.8	4.8	368.0	140.6	4,825.0	1,878	23.6	6.2
W41	Ca–HCO_3	BGW	$C1_{BGW}$	83.2	6.6	88.3	27.4	53.7	33.6	352.0	37.9	2.3	<D.L.	132.4	204.1	638	22.4	6.7
W42	Ca–HCO_3	BGW	$C1_{BGW}$	120.0	10.0	130.0	32.8	86.5	41.9	509.0	34.5	3.8	<D.L.	108.7	364.6	786	21.8	6.7
W43	Na–HCO_3	BGW	$C1_{BGW}$	66.0	2.9	909.0	236.0	202.0	696.0	1,510.0	62.6	8.8	386.0	437.0	9,186.3	3,880	47.7	7.0
W44	Na–HCO_3	BGW	$C1_{BGW}$	19.0	0.4	213.0	27.9	114.0	114.0	244.0	84.1	12.5	<D.L.	79.8	1,838.8	1,020	21.8	7.4
Min				3.7	0.1	43.8	20.6	28.3	5.1	48.8	<D.L.	0.4	<D.L.	<D.L.	191.3	350	16.4	5.7
Max				564.0	872.0	11,200.0	829.0	20,700.0	2,240.0	2,260.0	355.0	13.7	11,400.0	6,875.0	88,812.5	37,000	86.2	8.6
Average				143.9	51.9	1,567.8	172.8	2,278.7	409.7	757.6	56.3	5.0	2,026.5	561.3	8,260.1	6,469	34.1	7.0
CVR				89.9	115.5	108.1	86.6	100.5	83.5	76.7	145.1	75.4	148.2	125.7	130.9	87.6	44.4	8.4
GEW (Mofete 2)[c]				480	1	5,090	1,180	10,200	3,160	41	–	–	13,000	11,000	140,000	–	337	6.0
GEW (Mofete 1)[c]				555	–	10,025	1,230	17,710	615	81	–	–	25,000	9,000	125,000	–	250	7.5
GEW (Mofete 1)[c]				1,281	5	12,589	2,342	22,810	670	46	–	–	28,000	11,000	110,000	–	250	6.5
LSW[d]				447	1,397	12,250	446	22,390	2,906	161	–	–	170	2	4,410	–	20	8.1

<D.L.: below detection limit; CVR = (MAD/Median) × 100 where MAD is median absolute deviation (Reimann et al., 2008); GEW: geothermal water; LSW: local seawater. All values are in mg/l except for Li, As and B (μg/l), electric conductivity (EC; μS/cm), temperature (T; °C) and pH (unitless).

[a] The groups are based on the dominant anion species in meq/l: SGW, ClGW and BGW stand for sulfate-, chlorine- and bicarbonate-rich groundwater, respectively.

[b] The groups are based on hierarchical cluster analysis: $C1_{BGW}$, $C2_{MGW}$, $C3_{ClGW}$ and $C4_{SGW}$ denote the bicarbonate-rich, mixed, chlorine-rich and sulfate-rich groundwater, respectively.

[c] Guglielminetti (1986).

[d] Aiuppa et al. (2006).

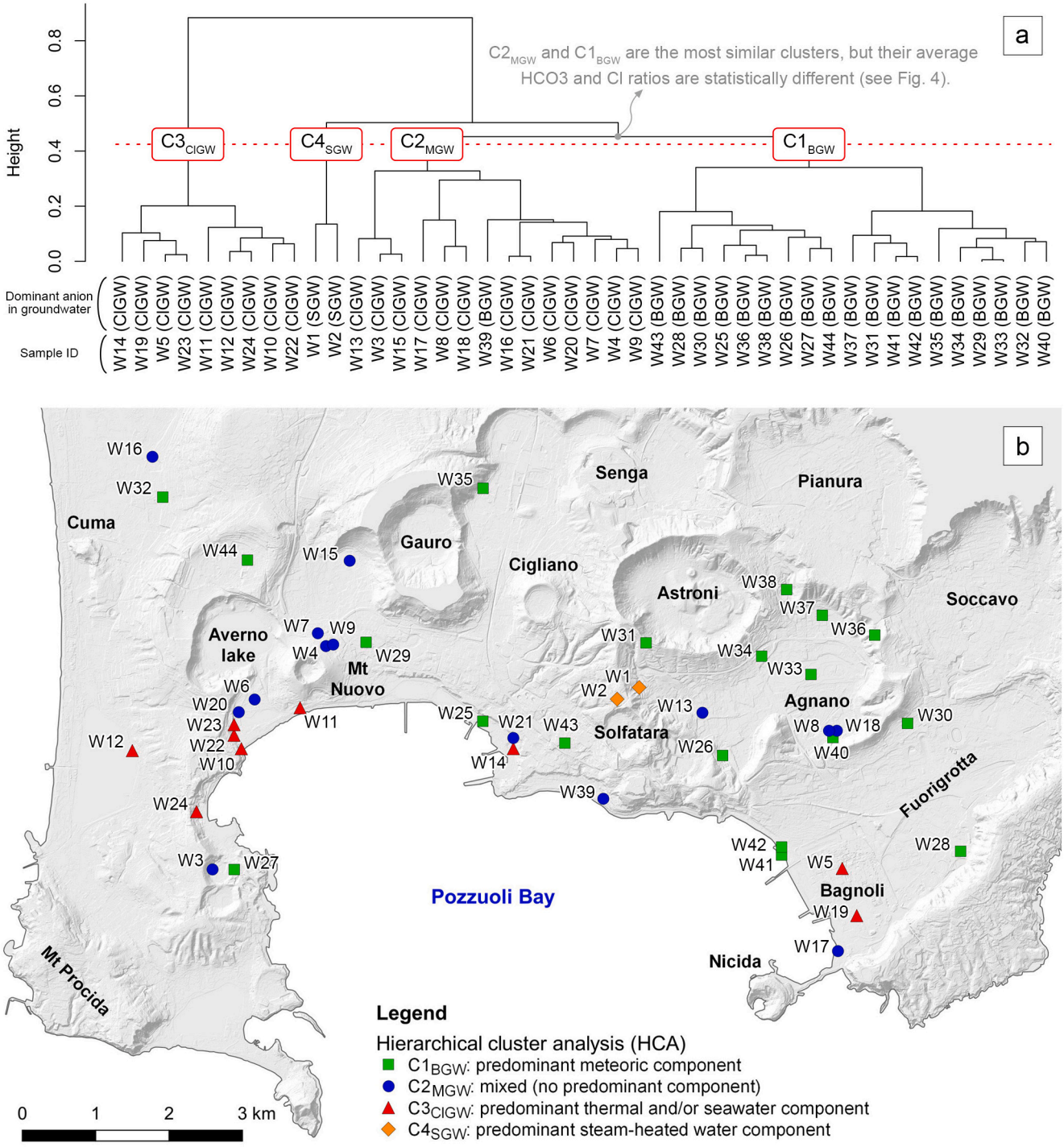

Fig. 3. (a) The dendrogram of hierarchical cluster analysis; and (b) spatial distribution of each group of groundwater samples. The height on the vertical axis of the dendrogram states the distance measure, indicating higher similarity at a lower value. On the horizontal axis of the dendrogram, BGW (bicarbonate-rich groundwater), ClGW (chlorine-rich groundwater) and SGW (sulfate-rich groundwater) refer to the dominant anion group. $C1_{BGW}$: bicarbonate-rich groundwater; $C2_{MGW}$: mixed groundwater; $C3_{ClGW}$: chlorine-rich groundwater; and $C4_{SGW}$: sulfate-rich groundwater.

2015). The recent uplift phase is still ongoing leading to significant variation in degassing rate, fumarolic composition and shallow earthquakes (Cardellini et al., 2017; Chiodini et al., 2010; Giudicepietro et al., 2019). Variations in pH, ammonia and/or SO_4^{2-}/Cl^- ratio in pools and wells around the Solfatara crater (Fig. 1) from 1990 to 1999 revealed that this area is the best site for monitoring the changes in the deep hydrothermal system and the activities of the underlying magma chamber (Valentino and Stanzione, 2004).

Little is known about the hydrologic system of Campi Flegrei volcano at the southwestern boundary of Campania Plain. A very complex stratigraphy was indicated by the wells drilled up to ca. 3 km depth for geothermal exploration in Mofete, S. Vito and Agnano areas (AGIP, 1987; Rosi and Sbrana, 1987). Tuff, lava and subordinate sedimentary rocks are followed by their thermometamorphic equivalents at ~2 km depth. The layers are impervious in more than a few hundred meters depth (also due to the self-sealing processes originating from circulation of hydrothermal fluids), except for the fractured zones (Capaldi et al., 1992). The complex subsurface geology significantly influences the

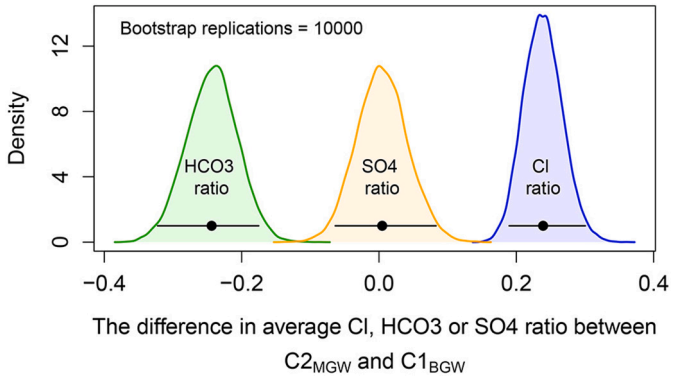

Fig. 4. Density plot of the difference in average HCO_3^-, SO_4^{2-} or Cl^- ratio between the mixed ($C2_{MGW}$) and bicarbonate-rich ($C1_{BGW}$) groundwater. The dots show the values obtained from the dataset in the present article and the horizontal line indicates the uncertainty based on the 95% confidence interval of 10,000 replications. In each bootstrap replication, for instance, average HCO_3^- ratio in the bicarbonate-rich groundwater is subtracted from that of the mixed groundwater. Thus, if the middle 95% of the distribution is different from zero, the difference is statistically significant.

shallow hydrologic system and leads to presence of superimposed aquifers in the study area. These aquifers, at a regional scale, can be considered as a unique aquifer due to horizontal discontinuities and geometrical variability of the lithotypes (Celico et al., 1987). The high piezometric level near Quarto plain (approximately 20 m a.s.l.; Fig. 1) is feasibly associated with deep fluids upwelling (Piochi et al., 2014) resulting in a pseudo-radial groundwater flow pattern at a regional scale. Accordingly, the groundwater flows towards the coastline in the southern, southeastern and western sectors, and towards the Campanian Plain aquifer in the northern sector (Fig. 1) (Celico et al., 1992; De Vita et al., 2018). Before reaching the sea, groundwater naturally emerges at the Averno volcanic lake, Lucrino, Fusaro and Miseno coastal lakes (Fig. 1) together with some thermal springs in Agnano plain and along the coast (Sellerino et al., 2019). The annual water-table fluctuation varies from 0.12 to 0.95 m, being the lowest in Agnano Plain. The time lag between precipitation and increase of water-table level ranges from 1 to 2 months in Quarto plain although there is an immediate correspondence in Agnano Plain. High water-table level was observed in the thermal wells of Damiani and Hotel Tennis (Fig. 1) 5 to 6 months after the timespan of major rainfall (Valentino and Stanzione, 2004).

Various origins were proposed for the thermal waters in Campi Flegrei: (1) Seawater or brines probably exist at depth that will be heated by the rising magmatic fluids (Dall'Aglio et al., 1972); (2) Local meteoric and deep hot marine components are mixed with different proportions (Baldi et al., 1975; Cortecci et al., 1978); (3) Thermal water and fumarolic steam mostly represent the meteoric origin (Bolognesi et al., 1986); (4) Thermal water and fumarolic steam are composed of a mixture of hot deep steam and local shallow water (Ghiara et al., 1988); (5) A shallow reservoir (depth <2,000 m) with seawater and local meteoric water origin, and a deep reservoir (depth >2,000 m) containing magmatic-meteoric hypersaline fluids feed the geothermal system of Campi Flegrei (Caprarelli et al., 1997). High As concentration in Na–Cl brines originates from prolonged water-rock interactions under reservoir temperature, fO_2 and fH_2S conditions, and the buffering effect of arsenopyrite–pyrite–pyrrhotite mineral assemblage. The brines are then diluted by As-depleted meteoric-derived groundwater during their ascent towards the surface and give rise to mixed waters with intermediate to low arsenic contents (Aiuppa et al., 2006). Regarding the gaseous composition of Solfatara fumaroles, Caliro et al. (2007) proposed two thermobarometric signatures at: (1) around 360 °C indicating the deep zone of hydrothermal system where CO_2-rich magmatic gases flash the hydrothermal fluid of meteoric origin (with fixed CO_2 fugacity due to fluid-rock interactions at high temperature) and form a gas plume; and (2) about 200–240 °C representing re-equilibration of the reactive species (i.e., H_2 and CO) in the rising gas plume. Extensive interaction of rocks with As-bearing hydrothermal steam results in intermediate to high As in the steam-heated groundwater (Aiuppa et al., 2006).

Valentino and Stanzione (2003) collected several water samples from 13 stations during 1994, considered the average major ion contents (literature data were included in some cases) and identified four end-members in Campi Flegrei: (1) alkali-chloride, highly saline water (Stufe di Nerone well and Stufe di Nerone spring); (2) alkali-bicarbonate, less saline water (Agnano spring and the water from Quarto plain); (3) alkali-bicarbonate-sulfate water (a sampling station in Quarto plain); and (4) alkaline earth-sulfate, acidic water (Pisciarelli Grande and Pisciarelli Piccola). They proposed that the groundwater from Pozzanghera Agnano Terme, Hotel Tennis, Terme Puteolane and Damiani is mixture of the end-members. However, Aiuppa et al. (2006) used the percent meq/l of HCO_3^-, SO_4^{2-} and Cl^-, defined the prevalent anion species and grouped 64 samples in bicarbonate-, chlorine- and sulfate-rich groundwater. The latter classification can be considered as the generalized version of the former, being beneficial when investigating a large number of samples.

3. Materials and methods

3.1. Sampling and chemical analysis

Majority of the published hydrogeochemical data in Campi Flegrei refer to specific monitoring points which are not suitable for the purpose of the present study because the samples do not cover the whole study area. In May–June 2002, sixty-four groundwater samples were collected and the analytical results were published (Aiuppa et al., 2006), but location and descriptive ID of each sampling point are not available. Therefore, in this study, a total of 44 water samples are collected in May 2019 from wells and springs mostly located in the NYT caldera (Fig. 1, Table S1). Alkalinity, electric conductivity (EC), pH and temperature are measured with portable instruments in situ. The water samples are filtered with 0.45 μm filters and collected in 30 ml high-density polyethylene (HDPE) bottles for chemical analyses. One aliquot is acidified (1%) with Suprapure 36% HCl for determination of the major cations, whereas the aliquot for minor and trace elements is acidified (1%) with Suprapure 63% HNO_3. Samples are analyzed for Li, Ca^{2+}, Mg^{2+}, Na^+, K^+, SO_4^{2-}, Cl^-, NO_3^- and F^- by ion chromatography standard technique, using a Dionex ICS3000 system at the laboratory of fluid geochemistry at the INGV-Osservatorio Vesuviano, Napoli. Measurement accuracy is better than ±5%, obtained by analyzing certified standard solutions, and the detection limits are better than 0.1 mg/l. Arsenic and boron contents are detected using inductively coupled plasma-optical emission spectrometry (ICP-OES) at the Department of Earth, Environmental and Resources Sciences in the University of Naples Federico II, following 0.45-μm filtration and HNO_3 acidification of another aliquot in the field. Measurement accuracy is better than ±5%, obtained by analyzing certified standard solutions, and the detection limits are 3.0 μg/l.

3.2. Statistical analysis

3.2.1. Hierarchical cluster analysis (HCA)

Most natural datasets are composed of several unknown subpopulations with specific characteristics (e.g., average, median and standard deviation). HCA is an exploratory statistical approach for uncovering these subgroups and creating homogeneous clusters in a dataset. The samples occurring in a cluster tend to have the highest possible similarity to each other, but the differences between the clusters are as large as possible. However, like factor analysis and principal component analysis, it cannot itself be a "statistical proof" of a certain relationship between samples and the corresponding groups (Reimann

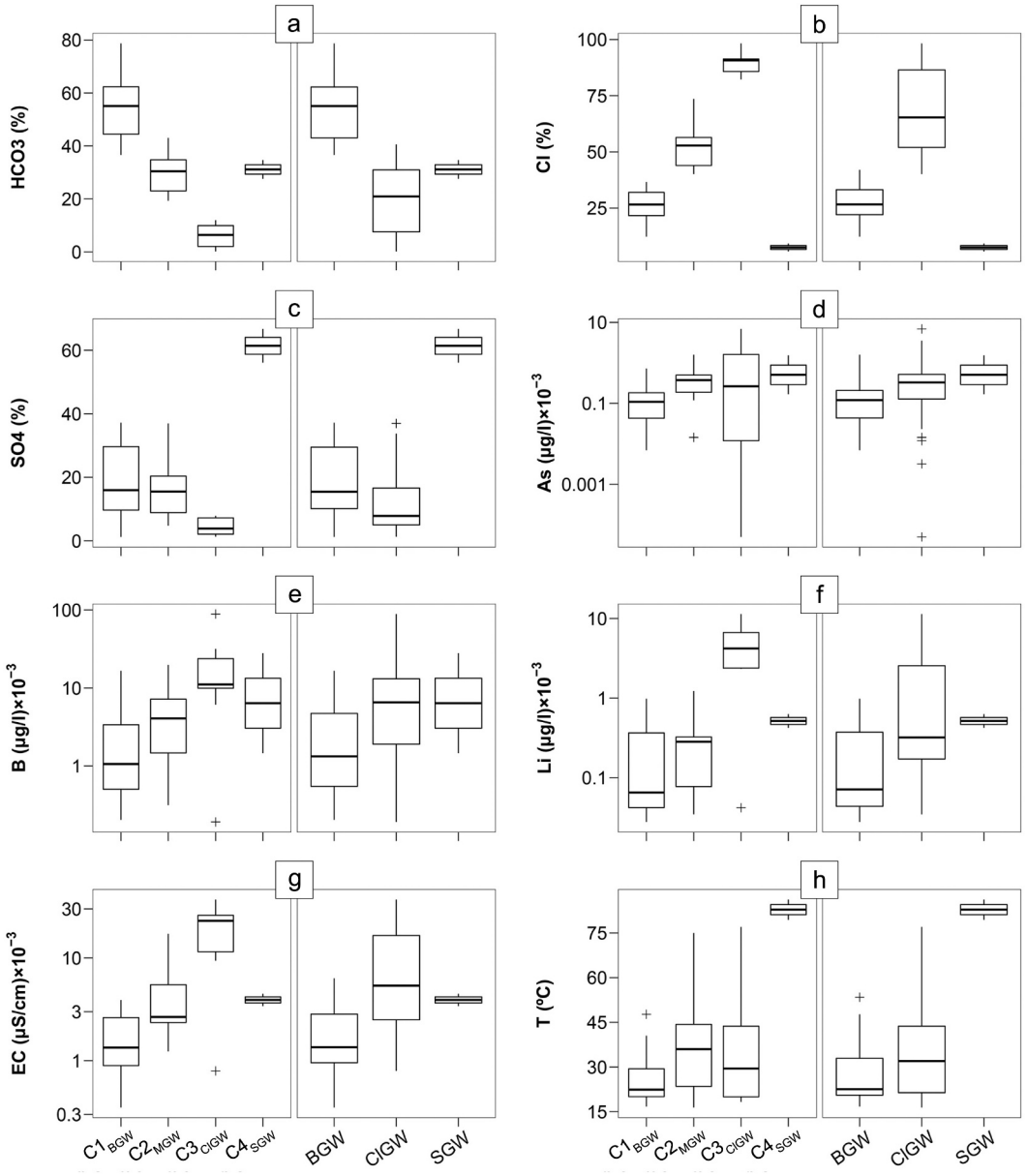

Fig. 5. Variation of selected parameters in the HCA groups and dominant anion groups (the left and right panels in each paired graph, respectively). To generate panels a to c, the following calculations are made using bicarbonate, chloride and sulfate in meq/l: $HCO_3^- = (HCO_3^-/(HCO_3^- + Cl^- + SO_4^{2-})) \times 100$; $Cl^- = (Cl^-/(HCO_3^- + Cl^- + SO_4^{2-})) \times 100$; and $SO_4^{2-} = (SO_4^{2-}/(HCO_3^- + Cl^- + SO_4^{2-})) \times 100$. Scale of y-axis is logarithmic in As, B, Li and EC (d to g, respectively) boxplots. EC stands for electric conductivity and the abbreviations on the horizontal axes are the same with Fig. 3.

et al., 2008). In HCA, a distance matrix is computed which explains the similarity degree between observations, and each observation is initially considered as an isolated group. Then, the two most similar ones are joined using an agglomeration technique and this process continues until all observations are pooled in a single group. The distances between clusters are recalculated at each stage depending on the selected method (Filzmoser et al., 2018; Keshavarzi et al., 2015; Van den Boogaart and Tolosana-Delgado, 2013). Euclidean measure is chosen to obtain the distance between the individuals and the McQuitty method (McQuitty, 1966) is applied as the agglomeration technique in the present article. The R package "stats" (R Core Team, 2021) is utilized to perform hierarchical clustering.

Variables with very different levels (e.g., major vs. trace elements) should not undergo HCA without proper data transformation and standardization, otherwise the variable with the highest variance affects the outcome noticeably. Including or excluding only one variable can also lead to completely different hierarchical clustering results (Reimann et al., 2008). In this study, ratios of bicarbonate, sulfate and chloride are considered for cluster analysis (Fig. 2) because the major ions could show the main processes regulating groundwater composition in Campi Flegrei (Aiuppa et al., 2006):

$$Cl^- \text{ ratio} = \frac{Cl^-}{HCO_3^- + SO_4^{2-} + Cl^-} \quad (1)$$

$$SO_4^{2-} \text{ ratio} = \frac{SO_4^{2-}}{HCO_3^- + SO_4^{2-} + Cl^-} \quad (2)$$

$$HCO_3^- \text{ ratio} = \frac{HCO_3^-}{HCO_3^- + SO_4^{2-} + Cl^-} \quad (3)$$

where all values are in mg/l. Presence of outliers and variance of the above-mentioned ratios are double-checked prior to hierarchical clus-

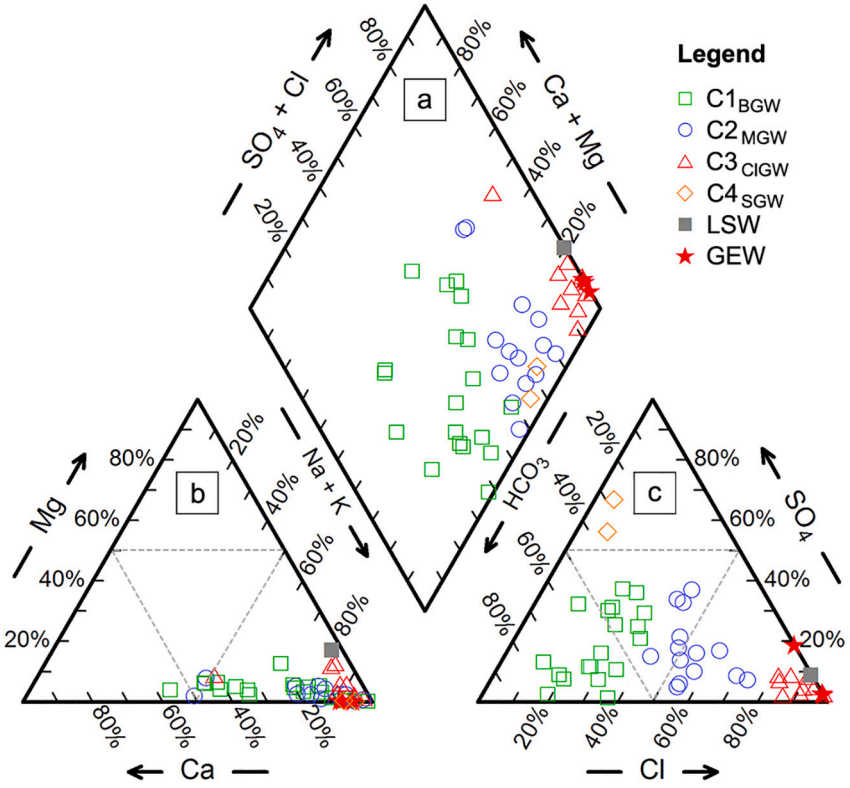

Fig. 6. Piper diagram showing composition of Campi Flegrei groundwater, grouped according to HCA results, together with geothermal water (GEW) and local seawater (LSW): (a) the diamond-shaped field; (b) the cation field; and (c) the anion field. The abbreviations in the legend are the same with Fig. 3.

tering (Fig. 2). Data outliers likely affect the distance measures and distort the data structure, but they need to be appropriately accommodated because they may signal some unexpected behavior in the hydrothermal system (Reimann et al., 2008).

3.2.2. Compositional data analysis

Majority of geochemical data are concentrations of constituents, relative in nature, depend on one another and sum up to a constant. These data are called compositional data and they are restricted to the positive part of the real sample space. Hence, their algebraic-geometric structure (i.e. the Aitchison geometry) is different from that of Euclidian geometry in real space. Applying traditional interpretive methods such as scatterplots and correlation analysis to data on the simplex can be misleading (Pearson, 1897; Kynčlová et al., 2017; Reimann et al., 2017). Compositional data analysis refers to the statistical approach that respects geometry of compositional data and helps for interpreting the relationships between relative components. The additive log-ratio (alr), centred log-ratio (clr) and isometric log-ratio (ilr) transformations were introduced by Aitchison (1982) and Egozcue et al. (2003) for solving the problem by converting a composition to a real vector prior to data elaboration in unconstrained conditions.

3.2.2.1. The isometric log-ratio (ilr)-ion plot. The Piper diagram was introduced in 1944 to classify different water types, characterize mixing of water masses and determine the chemical reactions regulating water chemistry in a set of water samples under investigation (Piper, 1944). Although application of the diagram has obviously been beneficial in the last eight decades, it has been challenging in some circumstances. For instance, distinguishing between waters mainly composed of Ca^{2+}, Mg^{2+}, SO_4^{2-} and Cl^- is difficult particularly for large datasets because of the structure of the diamond-shaped field in Piper diagram. Another issue is clustering the points along the boundaries and in the corners of the plot when water is concentrated in a particular pair of cation and anion. In order to overcome the above-mentioned shortcomings and improve the robustness of the Piper diagram, Shelton et al. (2018) used compositional data analysis and calculated four isometric log-ratios for the major chemical species of the original diagram as follows:

$$z_1 = \sqrt{\frac{2}{3}} ln \frac{\sqrt{[Ca^{2+}][Mg^{2+}]}}{[Na^+ + K^+]} \quad (4)$$

$$z_2 = \frac{1}{\sqrt{2}} ln \frac{[Ca^{2+}]}{[Mg^{2+}]} \quad (5)$$

$$z_3 = \sqrt{\frac{2}{3}} ln \frac{\sqrt{[Cl^-][SO_4^{2-}]}}{[HCO_3^- + CO_3^{2-}]} \quad (6)$$

and

$$z_4 = \frac{1}{\sqrt{2}} ln \frac{[Cl^-]}{[SO_4^{2-}]} \quad (7)$$

where all concentrations are in meq/l. The ilr-ion plot is then generated as a four-panel scatterplot (Fig. 2). Shelton et al. (2018) compared the Piper diagram and the proposed alternative diagram using multiple synthetic and real datasets and indicated that the latter offers a more in-depth assessment of water chemistry. The ilr-ion plot could be produced through the R code provided by Shelton et al. (2018).

3.2.2.2. Scatterplots. Generating scatterplots by raw or log-transformed data probably results in misinterpretation because of ignoring the compositional nature of the data (Reimann et al., 2017). Symmetric coordinates, a special case of isometric log-ratio transformation, is an option to solve this data problem by capturing all the relative information regarding the two compositional parts of interest (Kynčlová et al., 2017). In this study, symmetric coordinates and the frequently

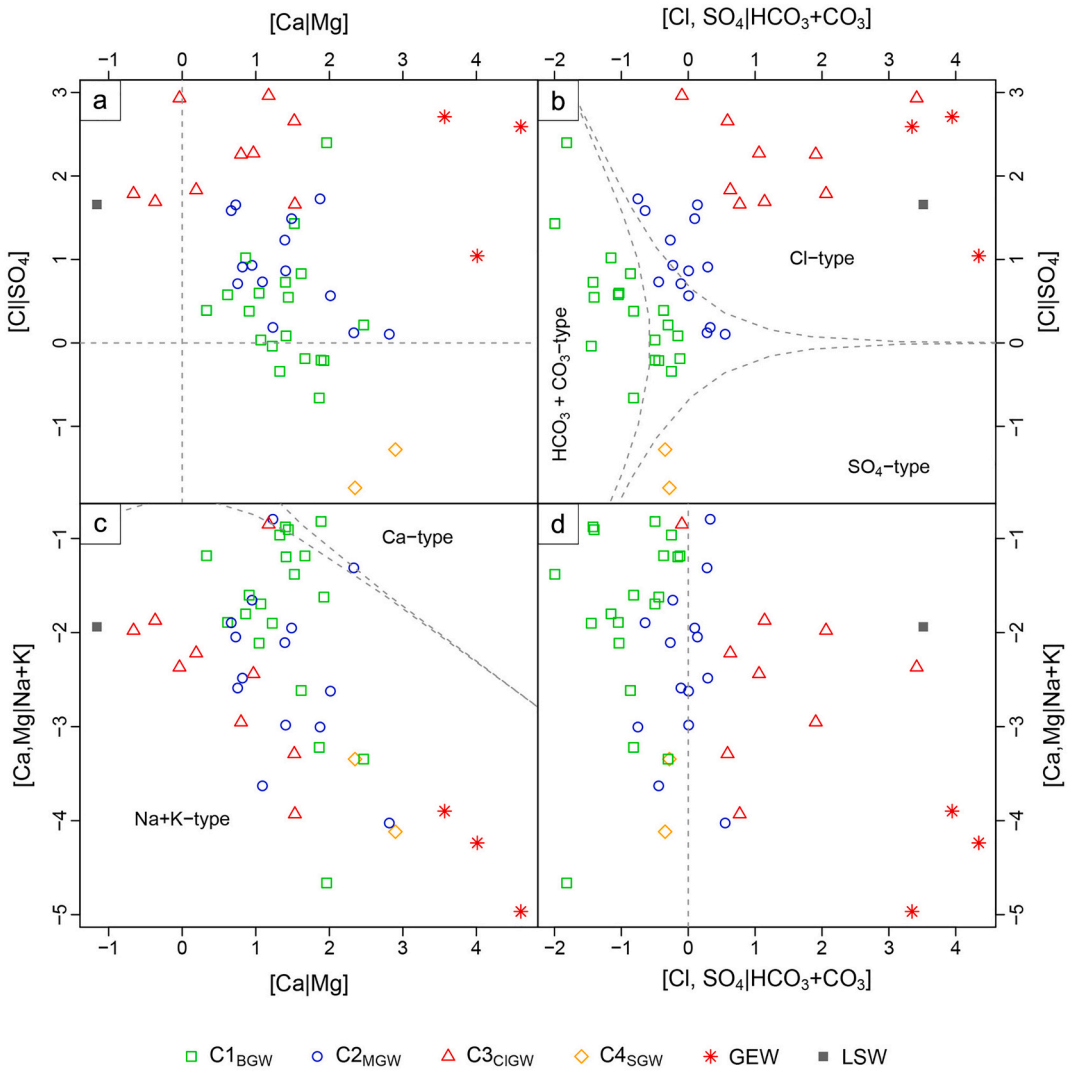

Fig. 7. Chemical composition of the collected groundwater samples on the ilr-ion plot: (a) the information in this panel is not specifically presented in the Piper diagram; (b) corresponds to the anion field of the Piper diagram; (c) corresponds to the cation field of the Piper diagram; and (d) corresponds to the diamond-shaped field of the Piper diagram. The abbreviations are the same with Fig. 3.

used classical log-transformation are chosen to investigate the importance of data closure (i.e. the constant sum constraint) (Fig. 2). Previous studies indicated that the former characterizes the relationships between elements better (e.g., Somma et al., 2021). The R package "robCompositions" (Filzmoser et al., 2018) is used for computing the symmetric coordinates in Figs. 8 and 9. The interested readers are referred to Kynčlová et al. (2017) for the calculation steps. Linear regression model is finally applied via the R package "ggpmisc" (Aphalo, 2021) and the coefficient of determination (R^2) is obtained for the selected parameters.

In addition, two isometric log-ratios were constructed with Na^+, Cl^- and HCO_3^- concentrations following the sequential binary partitioning procedure (Egozcue and Pawlowsky-Glahn, 2005). These coordinates are also called balances. Sodium and chloride are the major components of Na–Cl brines and seawater whilst bicarbonate is characteristic of meteoric water and CO_2-rich hydrothermal waters. Generating the following balance can describe the sources of Na^+ and Cl^- in comparison with those of HCO_3^-:

$$\left[Na^+, Cl^- | HCO_3^-\right] = \sqrt{\frac{2}{3}} ln \frac{\sqrt{[Na^+][Cl^-]}}{[HCO_3^-]} \quad (8)$$

where all values are in mg/l. The second balance also helps to assess relative variation of Na^+ and Cl^- for detecting the samples similar to Na–Cl brines and seawater:

$$[Na^+|Cl^-] = \frac{1}{\sqrt{2}} ln \frac{[Na^+]}{[Cl^-]} \quad (9)$$

where all concentrations are in mg/l. The R code for generating a scatterplot based on Eqs. (8) and (9) is available in supplementary material.

4. Results and discussion

In this section, groundwater samples are categorized in three groups based on the dominant anion species and in four groups regarding the results of hierarchical cluster analysis (Table 1). To avoid confusion, the abbreviations (i.e. BGW, ClGW and SGW which stand for bicarbonate-, chlorine- and sulfate-rich groundwater, respectively) are exclusively used for discussing the dominant anion groups. However, the HCA groups are *mainly* referred to as bicarbonate-rich, mixed, chlorine-rich and sulfate-rich groundwater ($C1_{BGW}$, $C2_{MGW}$, $C3_{ClGW}$ and $C4_{SGW}$, respectively).

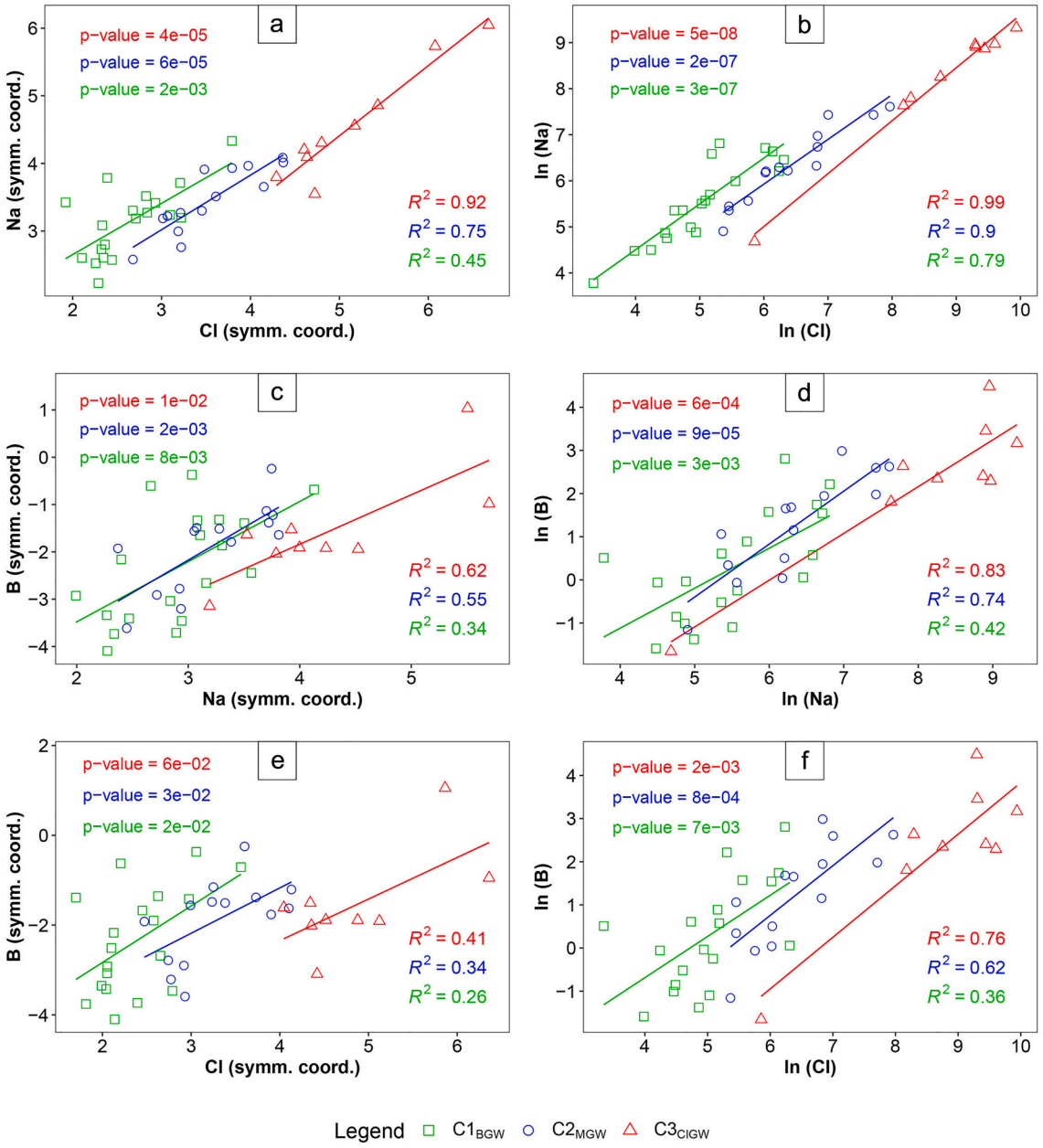

Fig. 8. The relationship between Na^+, Cl^- and B considering the symmetric coordinates (a, c and e) and the classical log-transformed data (b, d and f). The ions (Ca^{2+}, Mg^{2+}, Na^+, K^+, HCO_3^-, SO_4^{2-}, Cl^-, NO_3^- and F^-) as the main water components along with As, Li and B as the indicators of hydrothermal activity were used for calculation of the symmetric coordinates. The sulfate-rich groundwater is excluded because of few samples. The abbreviations in the legend are the same with Fig. 3.

4.1. An overview of groundwater composition

Na–Cl and Na–HCO_3 are the main groundwater types in Campi Flegrei (Table 1). However, Na–SO_4 is exclusive to the groundwater around Solfatara crater with the highest temperatures (>79 °C). On average, Na–Cl groundwater is 10 °C warmer than Na–HCO_3 groundwater. The average contents of cations and anions follow the orders of Na^+ (1,567.8 mg/l) > K^+ (172.8 mg/l) > Ca^{2+} (143.9 mg/l) > Mg^{2+} (51.9 mg/l) and Cl^- (2,278.7 mg/l) > HCO_3^- (757.6 mg/l) > SO_4^{2-} (409.7 mg/l) > NO_3^- (56.3 mg/l) > F^- (5.0 mg/l), respectively. Lithium, arsenic and boron show the highest robust coefficient of variation (CVR) which probably suggest their unique source. The pH values range from 5.7 in Na–Cl groundwater to 8.6 in Na–HCO_3 groundwater revealing the acidic to alkaline nature of the groundwaters under investigation. Nonetheless, electric conductivity indicates a reverse trend, decreasing from Na–Cl groundwater to Na–HCO_3 groundwater (Table 1).

Regarding the dominant anion groups in Table 1, BGW (T = 16.7 to 53.4 °C and EC = 350 to 6,340 μS/cm) mostly represents the meteoric-derived water which can be supported by the isotopic investigations of Caprarelli et al. (1997). Mixing this groundwater and Na–Cl brines (i.e. the chemically and isotopically modified seawater due to heating, boiling and interacting with rocks; Caprarelli et al. (1997)) leads to ClGW (T = 16.4 to 77 °C and EC = 795 to 37,000 μS/cm). On the other hand, the interaction between BGW and the vapor phase forms SGW with high temperature (>79 °C) and intermediate electric conductivity (3,400 to 4,480 μS/cm). Chiodini et al. (2001, 2003) reported high $H_2S_{(g)}$ in the condensing hydrothermal vapors. Oxidizing H_2S by atmospheric gases results in elevated sulfate concentration in the groundwater around Solfatara crater.

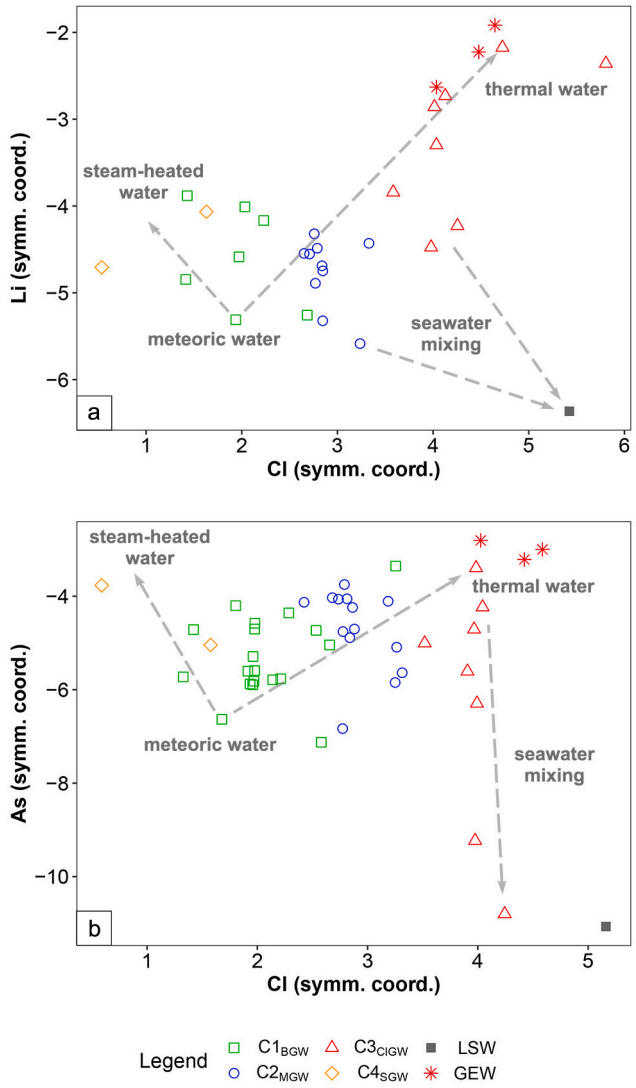

Fig. 9. Li–Cl^- and As–Cl^- scatterplots (a and b, respectively) generated by the symmetric coordinates. The ions (Ca^{2+}, Mg^{2+}, Na^+, K^+, HCO_3^-, SO_4^{2-} and Cl^-) as the main water components along with As, Li and B as the indicators of hydrothermal activity are used for calculation of the symmetric coordinates. The samples with a lithium content of below detection limit are excluded in the Li–Cl^- panel. The abbreviations in the legend are the same with Fig. 3.

4.2. Detection of homogeneous groundwater groups

Many data outliers are detected in Cl^- and SO_4^{2-} boxplots and variance of chloride is two orders of magnitude higher than those of bicarbonate and sulfate (Fig. S1a to c). However, computing the anion ratios alleviates these data problems for applying clustering algorithm (Fig. S1d to f). The collected samples can be categorized in the bicarbonate-rich, sulfate-rich, chlorine-rich and mixed groundwater based on Fig. 3. On average, the first two groups are spatially located far from the coastline, where the piezometric level is >1 m a.s.l. (Figs. 1 and 3 and Table S2). As the groundwater body flows towards the coast, the mixed and chlorine-rich groundwater become dominant. It is worth mentioning that the water from Agnano spring (W40 in Tables 1 and S1) is likely affected by magmatic CO_2 and buffered by water-rock interactions (Valentino and Stanzione, 2004), but it is grouped with the meteoric waters ($C1_{BGW}$) due to the similar bicarbonate, sulfate and chloride contents. Nevertheless, compared with the dominant anion groups, hierarchical cluster analysis divides ClGW into (Fig. 3):

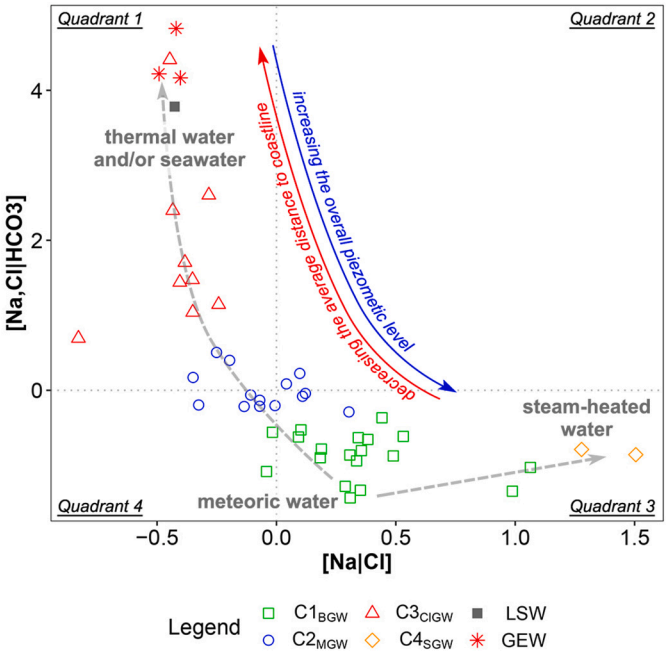

Fig. 10. The relationship between the isometric log-ratios computed using Na^+, Cl^- and HCO_3^- in mg/l. The abbreviations in the legend are the same with Fig. 3.

(1) *mixed groundwater* (*$C2_{MGW}$*). Valentino and Stanzione (2003) introduced the water samples collected in Pozzanghera Agnano Terme, Hotel Tennis, Terme Puteolane and Damiani as a mixture of the end-members. These samples occur in this group and consequently no predominant source (or a mixed source) is expected for the whole group. It is worth mentioning that bicarbonate is the dominant anion in Puteolane (W39 in Fig. 3), but HCA results express that it underwent a mixing process which is consistent with the measurements in the late 20th century (Table S3).

(2) *chlorine-rich groundwater* (*$C3_{ClGW}$*). The groundwater around Stufe di Nerone well and Stufe di Nerone spring, and the groundwater in Bagnoli coastal plain are present in this group. In Stufe di Nerone well, the deep geothermal component is hot "mature" seawater modified through water-rock interactions. Ammonium contents in the groundwater from Stufe di Nerone well and Stufe di Nerone spring also suggested a mixing process between deep geothermal and shallow meteoric components (Valentino and Stanzione, 2004). In addition, rise of hydrothermal fluids along fractures or faults was reported in the Bagnoli plain by Celico et al. (2001) and De Vivo and Lima (2008). Hence, the groundwater with predominant thermal and/or seawater component likely present in this group.

Although the mixed and bicarbonate-rich groundwaters are the highest similar groups, because they join together in Fig. 3a, the statistically significant difference in average Cl^- and HCO_3^- ratios between them reveals their effective clustering (Fig. 4). It is noteworthy that HCA considers the multivariate data space through calculating the distances between observations. Significance of difference in average of the ratios between other combinations of clusters is not assessed due to their few observations and limitation of the bootstrapping approach. The sulfate-rich groundwater is the next group that merges these two at a higher level of the dendrogram (Fig. 3a), probably showing a relatively stronger fingerprint of meteoric water in composition of groundwater in the study area, except for the chlorine-rich groundwater.

Chemical signature of the four groups of HCA versus the three groups

of dominant anion species are compared in Fig. 5. It is evident that the percentages of bicarbonate and sulfate (left panels in Fig. 5a and c) decrease from the meteoric end-member ($C1_{BGW}$) to the thermal/seawater end-member ($C3_{ClGW}$) although chloride percentage, arsenic, boron, lithium, electric conductivity and temperature (left panels in Fig. 5b, d, e, f, g and h, respectively) show a reverse trend. Values of the selected parameters in the mixed groundwater range between the corresponding values in bicarbonate- and chlorine-rich groundwater which confirm their hybrid nature. Compared to the bicarbonate-rich groundwater (As = 158.2 ± 169 μg/l, B = 2,875.3 ± 3,973 μg/l and EC = 1,732.1 ± 1,086 μS/cm), the average arsenic, boron and electric conductivity values are almost double in the mixed groundwater (As = 451.4 ± 388 μg/l, B = 5,955.1 ± 5,679 μg/l and EC = 4,482.9 ± 4,027 μS/cm) and one order of magnitude greater in the chlorine-rich groundwater (As = 1,457.8 ± 2,210 μg/l, B = 21,787.4 ± 25,278 μg/l and EC = 20,118.3 ± 11,138 μS/cm). The bicarbonate-rich groundwater is the coldest (25.6 ± 8 °C), but the chlorine-rich groundwater is the most acidic (pH = 6.6 ± 0.4; Table 1). The sulfate-rich groundwater has the lowest Cl^- (%), but the highest SO_4^{2-} (%) and temperature (Fig. 5b, c and h, respectively). The average arsenic, boron and electric conductivity values in this group (847.2 ± 679 μg/l, 14,678.8 ± 13,221 μg/l and 3,940.0 ± 540 μS/cm, respectively) lie between those of bicarbonate- and chlorine-rich groundwater. A part of this information cannot be obtained from categorizing the samples based on the dominant anion species (i.e. the right panels in Fig. 5a to h).

4.3. Compositional data analysis and hydrogeochemistry of volcanic aquifers

4.3.1. The hidden information in the major ions data

Composition of the four groundwater groups (i.e. $C1_{BGW}$, $C2_{MGW}$, $C3_{ClGW}$ and $C4_{SGW}$) is compared with chemistry of the geothermal fluid and local seawater through Piper diagram (Fig. 6) and ilr-ion plot (Fig. 7). A quick look at these two graphical approaches for analyzing water chemistry clarifies the advantages of utilizing the compositional alternative of the original Piper diagram. Regardless of the different isometric log-ratios in Fig. 7, the chlorine-rich groundwater is not condensed in the corners of the ilr-ion plot and their chemical variation can be assessed in detail.

Excluding the sulfate-rich groundwater, the positive correlation between the samples is better demonstrated in Fig. 7b. The bicarbonate-rich groundwater shows the lowest Cl^-/SO_4^{2-} together with Cl^- and SO_4^{2-} against $HCO_3^- + CO_3^{2-}$. Values of these ratios gradually increase in the mixed and chlorine-rich groundwater confirming higher contribution of seawater and/or Na–Cl brines. It is noteworthy that the greatest variation of $[Cl^-, SO_4^{2-} | HCO_3^- + CO_3^{2-}]$ is observed in the chlorine-rich groundwater whilst significant changes of $[Cl^- | SO_4^{2-}]$ is evident in the bicarbonate-rich groundwater (Fig. 7b). It might show the complex situation in the study area which cannot be detected in the original Piper diagram (Fig. 6c).

Although it is difficult to distinguish all groups in cation trilinear plot of the Piper diagram (Fig. 6b) due to significant data clustering, the data points are scattered in the ilr-ion plot (Fig. 7c) which allows to decipher the underlying hydrogeochemical interactions. The Ca^{2+}/Mg^{2+} log-ratio indicates the smallest value in seawater and increases with decreasing Ca^{2+} and Mg^{2+} versus $Na^+ + K^+$ in chlorine-rich groundwater (Fig. 7c). Neoformation of Mg-bearing clay minerals and dissolution of Na-rich vitreous volcanic rocks were previously proposed as the geochemical processes regulating the evolutionary trend of seawater (Valentino and Stanzione, 2003).

The lower-right panel of the ilr-ion plot (Fig. 7d) mimics the diamond-shaped field of the Piper diagram (Fig. 6a). Even though concentrations of Cl^- and SO_4^{2-} are equal to $HCO_3^- + CO_3^{2-}$ in the mixed groundwater, the bicarbonate-rich groundwater is enriched in bicarbonates. In accordance with seawater and thermal fluids, the chlorine-rich groundwater contains higher chloride and sulfate contents in comparison with bicarbonates. Further, the ratio of Ca^{2+} and Mg^{2+} versus $Na^+ + K^+$ represent the following decreasing order (Fig. 7d): $C1_{BGW} > C2_{MGW} > C3_{ClGW}$.

In the ilr-ion plot, Fig. 7a provides interesting information about the hydrothermal system. Most of the bicarbonate-rich groundwater samples are composed of equal chloride and sulfate contents. Their mixture with hydrothermal fluid and/or seawater results in increasing chloride, but steam-heating leads to elevated sulfate contents. Calcium concentration is higher than magnesium level in majority of the samples (Fig. 7a).

4.3.2. The relationship between selected variables

In order to present the importance of considering all relevant information in compositional data, strength of the relationship between Na^+–Cl^-, B–Cl^- and B–Na^+ is evaluated via symmetric coordinates and log-transformed values (Fig. 8). In the groundwater samples with significant contribution of seawater or the hydrothermal fluids, a higher correlation coefficient (i.e. a greater R^2 value) between the selected pairs of variables is expected. This is confirmed in Fig. 8 because the weakest and the strongest relationships exist between the pairs of variables in the bicarbonate- and chlorine-rich groundwater, respectively. The mixed groundwater represents a moderate R-squared value. It is noteworthy that the R^2 values are higher in Fig. 8b, d and f due to spurious correlation. For instance, approximately 80% ($p < 0.05$) of sodium variation is explained by chloride in the groundwater samples mainly derived from meteoric water ($C1_{BGW}$). It reduces to 45% ($p < 0.05$) when symmetric coordinates of Na^+ and Cl^- are utilized for the linear regression model which seems more reliable regarding the groundwater origin (Fig. 8a and b). Contrary to Fig. 8f, the B–Cl^- relationship in the chlorine-rich groundwater is not statistically significant in Fig. 8e which deserves further evaluation with a larger dataset.

Owing to the conservative geochemical behavior of Li, it can be a potential tracer of the ascending hot deep brines (Giggenbach, 1991). Furthermore, elevated As concentrations in the Cl^--bearing high temperature springs probably explain prolonged water-rock-magmatic gas interactions in reservoir conditions (Ballantyne and Moore, 1988). The Li–Cl^- and As–Cl^- relationships were investigated by Aiuppa et al. (2006) to explore geochemical evolution of groundwater in the study area. Hence, the compositional counterparts (i.e. symmetric coordinates) were utilized to assess the relationships in the true data structure. Lithium and arsenic evidently increase with respect to Cl^- from meteoric derived waters towards thermal waters (Fig. 9). The chlorine-rich groundwater can consequently be considered as the deep reservoir brine partially diluted with meteoric water. Depending on hydrogeology of the volcanic aquifer, Na–Cl brines may be noticeably diluted with poor Li and As meteoric waters and give rise to the mixed groundwater. Seawater contribution is likely a process explaining the deviation from the mixing trend between the bicarbonate- and chlorine-rich groundwater (Fig. 9). Arsenic enrichment around Solfatara crater (the sulfate-rich groundwater spatially occurs in this area) is indicative of significant As in the vapor phase, condensing at shallow depth and giving rise to the steam-heated groundwater. It is in agreement with almost high As values in the fumarolic condensates of Solfatara (As~3,000 μg/l in the alkaline condensate; Aiuppa et al., 2006).

Plotting the isometric log-ratios generated using Na^+, Cl^- and HCO_3^- evidently represents geochemical evolution of the groundwater (Fig. 10). The bicarbonate- and sulfate-rich groundwater occurs in quadrant 3 of the graph ($[Na^+ | Cl^-] > 0$ and $[Na^+, Cl^- | HCO_3^-] < 0$), but the chlorine-rich groundwater lies in quadrant 1 ($[Na^+ | Cl^-] < 0$ and $[Na^+, Cl^- | HCO_3^-] > 0$). Nevertheless, the mixed groundwater occurs around intersection of the grey dotted lines indicating that Na^+ is equal to Cl^- and the ratio of sodium and chloride against bicarbonate is one. The overall peizometric level (Fig. 1) and the average distance to coastline (Fig. 3; Table S2) decrease as moving from quadrant 3 to quadrant 1 (Fig. 10). It verifies that the bicarbonate-rich meteoric water flows towards the sea, interacts with the chlorine-rich thermal/seawater

end-member and gives rise to the mixed groundwater. The chlorine-rich groundwater is characterized by the highest variation of Na^+ and Cl^- versus HCO_3^- and the lowest variation of Na^+/Cl^-. Their Na^+/Cl^- values are similar to those of local seawater and geothermal water, increasing as contribution of meteoric-derived water and water-rock interactions increases. Low ratios of sodium and chloride against bicarbonate in steam-heated waters suggest their meteoric origin (Valentino and Stanzione, 2004).

Precursors of volcanic eruption are mainly identified via geochemical measurements regularly on the proximal emissions such as fumaroles, hot springs and volcanic lakes (Aiuppa et al., 2007; De Moor et al., 2016) or by geodetic and seismic monitoring (Patanè et al., 2003; Sparks, 2003; McNutt and Roman, 2015). However, the intermediate or remote hydrogeochemical monitoring of volcanoes are sometimes documented for identification the precursors (Armienta and De la Cruz-Reyna, 1995; Caracausi et al., 2003). Barbieri et al. (2021) recently indicated that the remote approach is likely easier and more reliable than sampling the proximal volcanic fluid emissions. They found an increase of B and Li concentrations before the 2014 Bárðarbunga eruption (~115 km from the monitoring station) and the 2018 M_w 5.0 earthquake (occurred ~80 km from the monitoring site) in central Iceland during the 2010–2018 groundwater monitoring. It indicates the ongoing investigation on finding better precursors of volcanic eruption through hydrogeochemical monitoring. Given the results of compositional data analysis in Figs. 7 to 10, the recent advances in statistical analysis deserve further attention to explore the full potential of groundwater hydrogeochemistry for delineating volcanic activity and the related seismic events. The new approaches might identify the most useful chemical variables that can validate the seismic and volcanic events over time, avoiding arbitrary selection of a hydrogeochemical precursor. This is of the utmost importance in active volcanic areas like Campi Flegrei, where densely populated areas are located inside and around craters.

5. Conclusion

Campi Felgrei is an active volcano that has been investigated for several decades to understand the history of volcanic activity and monitor volcanic unrest. Hydrogeochemical studies are one of the important lines of research that help for characterizing risk of eruption. The previous studies showed that hydrogeochemical processes in the volcanic aquifer could be preliminarily understood using the dominant anion species (i.e. bicarbonate, chloride and sulfate). In the present article, major ions, Li, As, B, pH, electric conductivity and temperature are determined in 44 groundwater samples that are spatially distributed over the whole study area. Ratios of the above-mentioned anions are considered to run HCA, the representative number of clusters is determined regarding the detailed hydrogeochemical investigations in the study area and four groups are identified: (1) bicarbonate-rich groundwater; (2) chlorine-rich groundwater; (3) sulfate-rich groundwater; and (4) mixed groundwater. The relationships between variables in each group is then explored using compositional data analysis and the classical methods. Compared with the Piper diagram, the ilr-ion plot represents variations in major ions more clearly. In addition, the R-squared values obtained from linear regression model do not show spurious correlation when respecting the compositional nature of geochemical data. The scatterplot generated via the isometric log-ratios constructed by Na^+, Cl^- and HCO_3^- also indicates that the bicarbonate-rich meteoric water flows towards the sea, interacts with the chlorine-rich thermal/seawater end-member and gives rise to the mixed groundwater. The rising hydrothermal vapor, however, increases sulfate and arsenic contents of the groundwater body around Solfatara crater. This article revealed some advantages of compositional data analysis, but applying this technique is recommended in future to highlight its potentials for mitigating volcanic risk more effectively.

CRediT authorship contribution statement

Pooria Ebrahimi: Conceptualization, Software, Formal analysis, Investigation, Visualization, Writing - Original Draft, Writing - Review & Editing; **Annalise Guarino**: Writing - Review & Editing; **Vincenzo Allocca**: Writing - Review & Editing; **Stefano Caliro**: Investigation, Resources, Validation, Writing - Review & Editing; **Rosario Avino**: Investigation; **Emanuela Bagnato**: Investigation, Writing - Review & Editing; **Francesco Capecchiacci**: Investigation, Writing - Review & Editing; **Antonio Carandente**: Investigation; **Carmine Minopoli**: Investigation; **Alessandro Santi**: Investigation; **Stefano Albanese**: Resources, Supervision, Project administration, Writing - Review & Editing.

Declaration of competing interest

The authors declare that they have no known competing financial interests or personal relationships that could have appeared to influence the work reported in this paper.

Acknowledgement

The authors would like to thank Salvatore Dominech from School of Ocean and Earth Science at Tongji University (Shanghai, China) and Antonio Aruta from Department of Earth, Environmental and Resources Sciences at the University of Naples Federico II (Naples, Italy) for sharing ideas on application of compositional data analysis. We wish to express our gratitude to the associate editor and the anonymous reviewers for their constructive comments.

Funding

This research did not receive any specific grant from funding agencies in the public, commercial, or not-for-profit sectors.

Appendix A. Supplementary data

Supplementary data to this article can be found online at https://doi.org/10.1016/j.gexplo.2021.106922.

References

AGIP, 1987. Modello geotermico del sistemaflegreo. Sintesi, SEG-MESG Internal Report, 23 pp.

Aitchison, J., 1982. The statistical analysis of compositional data. J. R. Stat. Soc. Ser. B Methodol. 44 (2), 139–177.

Aiuppa, A., Avino, R., Brusca, L., Caliro, S., Chiodini, G., D'Alessandro, W., Favara, R., Federico, C., Ginevra, W., Inguaggiato, S., Longo, M., Pecoraino, G., Valenza, M., 2006. Mineral control of arsenic content in thermal waters from volcano-hosted hydrothermal systems: insights from island of Ischia and Phlegrean Fields (Campanian Volcanic Province, Italy). Chem. Geol. 229 (4), 313–330.

Aiuppa, A., Moretti, R., Federico, C., Giudice, G., Gurrieri, S., Liuzzo, M., Papale, P., Shinohara, H., Valenza, M., 2007. Forecasting Etna eruptions by real-time observation of volcanic gas composition. Geology 35, 1115–1118.

Allocca, V., Coda, S., De Vita, P., Di Rienzo, B., Ferrara, L., Giarra, A., Mangoni, O., Stellato, L., Trifuoggi, M., Arienzo, M., 2018. Hydrogeological and hydrogeochemical study of a volcanic-sedimentary coastal aquifer in the archaeological site of Cumae (Phlegraean Fields, southern Italy). J. Geochem. Explor. 185, 105–115.

Aphalo, P.J., 2021. ggpmisc: miscellaneous extensions to 'ggplot2'. R package version 0.3.9. https://CRAN.R-project.org/package=ggpmisc.

Arienzo, M., Allocca, V., Manna, F., Trifuoggi, M., Ferrara, L., 2015. Effectiveness of a physical barrier for contaminant control in an unconfined coastal plain aquifer: the case study of the former industrial site of Bagnoli (Naples, southern Italy). Environ. Monit. Assess. 187 (12), 761.

Armienta, M.A., De la Cruz-Reyna, S., 1995. Some hydro-geochemical fluctuations observed in Mexico related to volcanic activity. Appl. Geochem. 10 (2), 215–227.

Armienti, P., Barberi, F., Bizojard, H., Clocchiatti, R., Innocenti, F., Metrich, N., Rosi, M., Sbrana, A., 1983. The Phlegraean Fields: magma evolution within a shallow chamber. J. Volcanol. Geotherm. Res. 17 (1–4), 289–311.

Avino, R., Capaldi, G., Pece, R., 1999. Radon in active volcanic areas of Southern Italy. Il Nuovo Cimento C 22 (3-4), 379–386.

Bagnato, E., Parello, F., Valenza, M., Caliro, S., 2009. Mercury content and speciation in the Phlegrean Fields volcanic complex: evidence from hydrothermal system and fumaroles. J. Volcanol. Geotherm. Res. 187 (3–4), 250–260.
Baldi, P., Ferrara, G.C., Panichi, C., 1975. Geothermal research in western Campania, southern Italy: chemical and isotopic studies of thermal fluids in the Campi Flegrei. In: Proc. 2nd U.N. Symp. on Development and Use of Geothermal Resources, San Francisco, Vol. 1, pp. 687–697.
Ballantyne, J.M., Moore, J.N., 1988. Arsenic geochemistry in geothermal systems. Geochim. Cosmochim. Acta 52 (2), 475–483.
Barbieri, M., Franchini, S., Barberio, M.D., Billi, A., Boschetti, T., Giansante, L., Gori, F., Jónsson, S., Petitta, M., Skelton, A., Stockmann, G., 2021. Changes in groundwater trace element concentrations before seismic and volcanic activities in Iceland during 2010–2018. Sci. Total Environ. 793, 148635.
Bolognesi, L., Noto, P., Nuti, S., 1986. In: Studio chimico ed isotopico della Solfatara di Pozzuoli: ipotesi sull'origine e sulle temperature profonde dei fluidi, 41. Rendiconti della Societa Italiana di Mineralogia e Petrologia, pp. 281–295.
Buccianti, A., Grunsky, E., 2014. Compositional data analysis in geochemistry: are we sure to see what really occurs during natural processes? J. Geochem. Explor. 1–5 https://doi.org/10.1016/j.gexplo.2014.03.022.
Caliro, S., Chiodini, G., Moretti, R., Avino, R., Granieri, D., Russo, M., Fiebig, J., 2007. The origin of the fumaroles of La Solfatara (Campi Flegrei, South Italy). Geochim. Cosmochim. Acta 71 (12), 3040–3055.
Capaldi, G., Pece, R., Veltri, C., 1992. Radon variation in groundwaters in the Campi Flegrei Caldera (southern Italy) during and after the 1982–1984 bradyseismic crisis. Pure Appl. Geophys. 138 (1), 77–93.
Caprarelli, G., Tsutsumi, M., Turi, B., 1997. Chemical and isotopic signatures of the basement rocks from the Campi Flegrei geothermal field (Naples, southern Italy): inferences about the origin and evolution of its hydrothermal fluids. J. Volcanol. Geotherm. Res. 76 (1–2), 63–82.
Caracausi, A., Italiano, F., Paonita, A., Rizzo, A., Nuccio, P.M., 2003. Evidence of deep magma degassing and ascent by geochemistry of peripheral gas emissions at Mount Etna (Italy): assessment of the magmatic reservoir pressure. J. Geophys. Res. Solid Earth 108 (B10).
Cardellini, C., Chiodini, G., Frondini, F., Avino, R., Bagnato, E., Caliro, S., Lelli, M., Rosiello, A., 2017. Monitoring diffuse volcanic degassing during volcanic unrests: the case of Campi Flegrei (Italy). Sci. Rep. 7 (1), 1–15.
Celico, P., De Gennaro, M., Pagano, D., Ronca, A., Stanzione, D., Vallario, A., 1987. In: Idrogeologia e idrogeochimica dei Campi Flegrei: relazioni tra chimismo delle acque e idrodinamica sotterranea, Atti Convegno "Bradisismo e fenomeni connessi", Napoli, 19-20 gennaio 1987, pp. 94–100.
Celico, P., Dall'Aglio, M., Ghiara, M.R., Stanzione, D., Brondi, M., 1992. Geochemical monitoring of the thermal fluids in the phlegraean fields from 1970 to 1990. Boll. Soc. Geol. Ital. 111 (3–4), 409–422.
Celico, F., Esposito, L., Mancuso, M., 2001. Hydrodynamic and hydrochemical complexity of Naples urban area: some interpretations. Geol. Tec. Ambient. 2, 35–54.
Chandrasekharam, D., Bundschuh, J., 2002. Geochemistry of thermal waters and thermal gases. In: Chandrasekharam, D., Bundschuh, J. (Eds.), Geothermal Energy Resources for Developing Countries. Swets & Zeitlinger Publishers, Lisse, The Netherlands, pp. 253–267.
Chiodini, G., Frondini, F., Cardellini, C., Granieri, D., Marini, L., Ventura, G., 2001. CO2 degassing and energy release at Solfatara volcano, Campi Flegrei, Italy. J. Geophys. Res. Solid Earth 106 (B8), 16213–16221.
Chiodini, G., Todesco, M., Caliro, S., Del Gaudio, C., Macedonio, G., Russo, M., 2003. Magma degassing as a trigger of bradyseismic events: the case of Phlegrean Fields (Italy). Geophys. Res. Lett. 30 (8).
Chiodini, G., Caliro, S., Cardellini, C., Granieri, D., Avino, R., Baldini, A., Donnini, M., Minopoli, C., 2010. Long-term variations of the Campi Flegrei, Italy, volcanic system as revealed by the monitoring of hydrothermal activity. J. Geophys. Res. Solid Earth 115 (B3).
Chiodini, G., Caliro, S., De Martino, P., Avino, R., Gherardi, F., 2012. Early signals of new volcanic unrest at Campi Flegrei caldera? Insights from geochemical data and physical simulations. Geology 40 (10), 943–946.
Cortecci, G., Noto, P., Panichi, C., 1978. Environmental isotopic study of the Campi Flegrei (Naples, Italy) geothermal field. J. Hydrol. 36 (1–2), 143–159.
D'Auria, L., Pepe, S., Castaldo, R., Giudicepietro, F., Macedonio, G., Ricciolino, P., Tizzani, P., Casu, F., Lanari, R., Manzo, M., Martini, M., Sansosti, E., Zinno, I., 2015. Magma injection beneath the urban area of Naples: a new mechanism for the 2012–2013 volcanic unrest at Campi Flegrei caldera. Sci. Rep. 5, 13100.
Dall'Aglio, M., Martini, M., Tonani, F., 1972. In: Rilevamento geochimico delle emanazioni vulcaniche dei Campi Flegrei, Quaderni De 'La Ricerca Scientifica', 83. CNR, pp. 152–181.
De Moor, J.M., Aiuppa, A., Pacheco, J., Avard, G., Kern, C., Liuzzo, M., Martínez, M., Giudice, G., Fischer, T.P., 2016. Short-period volcanic gas precursors to phreatic eruptions: insights from Poás Volcano, Costa Rica. Earth Planet. Sci. Lett. 442, 218–227.
De Vita, P., Allocca, V., Celico, F., Fabbrocino, S., Mattia, C., Monacelli, G., Musilli, I., Piscopo, V., Scalise, A.R., Summa, G., Tranfaglia, G., Celico, P., 2018. Hydrogeology of continental southern Italy. J. Maps 14 (2), 230–241. https://doi.org/10.1080/17445647.2018.1454352.
De Vivo, B., Lima, A., 2008. Characterization and remediation of a brownfield site: the Bagnoli case in Italy. In: De Vivo, B., Belkin, H.E., Lima, A. (Eds.), Environmental Geochemistry. Site Characterization. Data Analysis and Case Histories. Elsevier, The Netherland, Amsterdam, pp. 356–384.
Del Gaudio, C., Aquino, I., Ricciardi, G.P., Ricco, C., Scandone, R., 2010. Unrest episodes at Campi Flegrei: a reconstruction of vertical ground movements during 1905–2009. J. Volcanol. Geotherm. Res. 195 (1), 48–56.
Di Girolamo, P., 1978. Geotectonic settings of Miocene-Quaternary volcanism in and around the eastern Tyrrhenian Sea border (Italy) as deduced from major element geochemistry. Bull. Volcanol. 41 (3), 229–250.
Dominech, S., Yang, S., Ebrahimi, P., Aruta, A., Guarino, A., Gramazio, A., Albanese, S., 2021. A new approach to determine geochemical fingerprint of contaminants in stream sediments of southern Italy. In: Goldschmidt2021• Virtual• 4-9 July.
Dominech, S., Yang, S., Aruta, A., Gramazio, A., Albanese, S., 2022. Multivariate analysis of dilution-corrected residuals to improve the interpretation of geochemical anomalies and determine their potential sources: the Mingardo River case study (Southern Italy). J. Geochem. Explor. 232, 106890.
Dotsika, E., 2015. H-O–C–S isotope and geochemical assessment of the geothermal area of Central Greece. J. Geochem. Explor. 150, 1–15.
Ebrahimi, P., Albanese, S., Esposito, L., Zuzolo, D., Cicchella, D., 2021. Coupling compositional data analysis (CoDA) with hierarchical cluster analysis (HCA) for preliminary understanding of the dynamics of a complex water distribution system: the Naples (South Italy) case study. Environ. Sci.: Water Res. Technol. 7 (6), 1060–1077.
Egozcue, J.J., Pawlowsky-Glahn, V., 2005. Groups of parts and their balances in compositional data analysis. Math. Geol. 37 (7), 795–828.
Egozcue, J.J., Pawlowsky-Glahn, V., Mateu-Figueras, G., Barcelo-Vidal, C., 2003. Isometric logratio transformations for compositional data analysis. Math. Geol. 35 (3), 279–300.
Filzmoser, P., Hron, K., Templ, M., 2018. Applied Compositional Data Analysis. Springer International Publishing. https://doi.org/10.1007/978-3-319-96422-5.
Ghiara, M.R., Stanzione, D., Bellucci, L., Panichi, C., 1988. Preliminary observations on the chemical variations of the solutes monitored in the thermal waters of the Phlegraean Fields in the period 1983–1985. Rend. Soc. Ital. Mineral. Petrol. 43, 1139–1150.
Giggenbach, W.F., 1991. Chemical techniques in geothermal exploration (co-ordinator). In: D'Amore, F. (Ed.), Application of Geochemistry in Geothermal Reservoir Development. UNITAR, pp. 119–144.
Giudicepietro, F., Chiodini, G., Caliro, S., De Cesare, W., Esposito, A.M., Galluzzo, D., Lo Bascio, D., Macedonio, G., Orazi, M., Ricciolino, P., Vandemeulebrouck, J., 2019. Insight into Campi Flegrei caldera unrest through seismic tremor measurements at Pisciarelli fumarolic field. Geochem. Geophys. Geosyst. 20 (11), 5544–5555.
Guglielminetti, M., 1986. Mofete geothermal field. Geothermics 15 (5–6), 781–790.
ISPRA (Istituto superiore per la protezione e la ricerca ambientale), 2018. Carta Geologica d'Italia. 1:50,000 Sheets: 446-447 Napoli.
Keshavarzi, B., Ebrahimi, P., Moore, F., 2015. A GIS-based approach for detecting pollution sources and bioavailability of metals in coastal and marine sediments of Chabahar Bay, SE Iran. Geochemistry 75 (2), 185–195. https://doi.org/10.1016/j.chemer.2014.11.003.
Kynčlová, P., Hron, K., Filzmoser, P., 2017. Correlation between compositional parts based on symmetric balances. Math. Geosci. 49 (6), 777–796.
McNutt, S.R., Roman, D.C., 2015. Volcanic seismicity. In: The Encyclopedia of Volcanoes. Academic Press, pp. 1011–1034. https://doi.org/10.1016/B978-0-12-385938-9.00059-6.
McQuitty, L.L., 1966. Similarity analysis by reciprocal pairs for discrete and continuous data. Educ. Psychol. Meas. 26 (4), 825–831. https://doi.org/10.1177/001316446602600402.
Moeck, I.S., 2014. Catalog of geothermal play types based on geologic controls. Renew. Sust. Energ. Rev. 37, 867–882.
Patanè, D., De Gori, P., Chiarabba, C., Bonaccorso, A., 2003. Magma ascent and the pressurization of Mount Etna's volcanic system. Science 299, 2061–2063.
Pearson, K., 1897. Mathematical contributions to the theory of evolution.—on a form of spurious correlation which may arise when indices are used in the measurement of organs. Proc. R. Soc. Lond. 60 (359-367), 489–498.
Peccerillo, A., 1985. Roman comagmatic province (central Italy): evidence for subduction-related magma genesis. Geology 13 (2), 103–106.
Piochi, M., Kilburn, C.R.J., Di Vito, M.A., Mormone, A., Tramelli, A., Troise, C., De Natale, G., 2014. The volcanic and geothermally active Campi Flegrei caldera: an integrated multidisciplinary image of its buried structure. Int. J. Earth Sci. 103 (2), 401–421.
Piper, A.M., 1944. A graphic procedure in the geochemical interpretation of water-analyses. EOS Trans. Am. Geophys. Union 25 (6), 914–928.
R Core Team, 2021. R: a language and environment for statistical computing. R Foundation for Statistical Computing, Vienna, Austria. https://www.R-project.org/.
Reimann, C., Filzmoser, P., Garrett, R., Dutter, R., 2008. Statistical Data Analysis Explained: Applied Environmental Statistics With R. John Wiley & Sons, West Sussex, England.
Reimann, C., Filzmoser, P., Hron, K., Kynčlová, P., Garrett, R.G., 2017. A new method for correlation analysis of compositional (environmental) data–a worked example. Sci. Total Environ. 607, 965–971.
Rosi, M., Sbrana, A., 1987. Phlegraean Fields, Quaderni de "La ricerca scientifica", Consiglio Nazionale delle Ricerche, 9, 175 pp.
Scarpati, C., Perrotta, A., Lepore, S., Calvert, A., 2013. Eruptive history of Neapolitan volcanoes: constraints from 40Ar–39Ar dating. Geol. Mag. 150 (3), 412–425.
Sellerino, M., Forte, G., Ducci, D., 2019. Identification of the natural background levels in the Phlaegrean fields groundwater body (Southern Italy). J. Geochem. Explor. 200, 181–192.
Shelton, J.L., Engle, M.A., Buccianti, A., Blondes, M.S., 2018. The isometric log-ratio (ilr)-ion plot: a proposed alternative to the Piper diagram. J. Geochem. Explor. 190, 130–141.

Somma, R., Ebrahimi, P., Troise, C., De Natale, G., Guarino, A., Cicchella, D., Albanese, S., 2021. The first application of compositional data analysis (CoDA) in a multivariate perspective for detection of pollution source in sea sediments: the Pozzuoli Bay (Italy) case study. Chemosphere 274, 129955.

Sparks, R.S.J., 2003. Forecasting volcanic eruptions. Earth Planet. Sci. Lett. 210 (1–2), 1–15.

Stellato, L., Coda, S., Arienzo, M., De Vita, P., Di Rienzo, B., D'Onofrio, A., Ferrara, L., Marzaioli, F., Trifuoggi, M., Allocca, V., 2020. Natural and anthropogenic groundwater contamination in a coastal volcanic-sedimentary aquifer: the case of the archaeological site of Cumae (Phlegraean Fields, Southern Italy). Water 12 (12), 3463.

Trasatti, E., Polcari, M., Bonafede, M., Stramondo, S., 2015. Geodetic constraints to the source mechanism of the 2011–2013 unrest at Campi Flegrei (Italy) caldera. Geophys. Res. Lett. 42 (10), 3847–3854.

Valentino, G.M., Stanzione, D., 2003. Source processes of the thermal waters from the Phlegraean Fields (Naples, Italy) by means of the study of selected minor and trace elements distribution. Chem. Geol. 194 (4), 245–274.

Valentino, G.M., Stanzione, D., 2004. Geochemical monitoring of the thermal waters of the Phlegraean Fields. J. Volcanol. Geotherm. Res. 133 (1–4), 261–289.

Valentino, G.M., Cortecci, G., Franco, E., Stanzione, D., 1999. Chemical and isotopic compositions of minerals and waters from the Campi Flegrei volcanic system, Naples, Italy. J. Volcanol. Geotherm. Res. 91 (2–4), 329–344.

Van den Boogaart, K.G., Tolosana-Delgado, R., 2013. Analyzing Compositional Data With R, Vol. 122. Springer, Berlin. https://doi.org/10.1007/978-3-642-36809-7.

Vitale, S., Isaia, R., 2014. Fractures and faults in volcanic rocks (Campi Flegrei, southern Italy): insight into volcano-tectonic processes. Int. J. Earth Sci. 103 (3), 801–819.

Washington, H.S., 1906. In: The Roman Comagmatic Region, Vol. 57. Carnegie Inst. of Washington, p. 199.